RAPID MODELLING OF MULTI-STEPPED ROTOR DYNAMICS

by
HAKAN KESKİN

Submitted to the Graduate School of Engineering and Natural Sciences
in partial fulfillment of
the requirements for the degree of
Master of Science

SABANCI UNIVERSITY
Spring 2004

RAPID MODELLING OF MULTI-STEPPED ROTOR DYNAMICS

APPROVED BY:

Associate Prof. Dr. ERHAN BUDAK .....
(Dissertation Advisor)

Assistant Prof. Dr. SERHAT YEŞİLYURT .....
(Dissertation Co-Advisor)

Prof. Dr. ASIF ŞABANOVİÇ .....

Assistant Prof. Dr. KEMALETTİN ERBATUR .....

Assistant Prof. Dr. AYHAN BOZKURT .....

DATE OF APPROVAL: .....

ABSTRACT

The major objective of the studies on the dynamic behaviour of rotors is to allow development of rotating machinery that will be free from vibrational problems. Rotor dynamics prediction has several important consequences for a large group of machinery. First of all, there are many machines with rotating components, i.e. rotors, such as turbines, compressors and pumps, machine tools, helicopters, dentist's tooth grinders etc. The dynamics of these systems are very critical for their proper functioning, stability, efficiency and health. For example, if one of the natural frequencies is in the operation region of the system, i.e. one of the excitation frequencies during the operation is close to one of the natural frequencies, then the system may resonate and the resulting large amplitude vibrations will cause loss of accuracy and efficiency in the operation, and may also damage the bearings and the rest of the machinery.

There are two main approaches to rotor dynamics analysis. For existing rotors, the dynamics can be measured using experimental techniques such as modal analysis. Although this can be a fast approach, it requires the experimental set up be available. Also, if there are many different components added to the rotor, such as different tool holders and tools on a machine tool spindle, then the measurements must be repeated for each combination which may result in high number of tests and waste of productive time on the machine. Prediction of the rotor dynamics during the design is another critical case where dynamics analysis is required. Obviously, testing is not a possible technique for this case. FEA can be used for the prediction of the dynamics. This may be a viable solution in many cases, however the bearing contact parameters, i.e. stiffness and damping, must be known in order to develop the model. Also, many simulations have to be performed for optimal design resulting in highest dynamic rigidity with smallest possible rotary inertia. This is usually very time consuming, and the optimal configuration may never be obtained.

The objective of this study is to develop a fast method for the dynamic analysis of rotor-bearing systems so that they can be used during the design and the operation of the machinery. The method can be used to determine the frequency response function of the system at critical locations for different geometric configurations very fast so that the design could be optimized. The effects and optimal values of some internal system parameters such as bearing preloads could also be determined using the method. Also, the dynamic response of the system could be updated after new components are added to the rotor.

ÖZET

Rotorların dinamik davranışı üzerine yapılan çalışmaların ana amacı titreşim problemlerine maruz kalmayan dönen makinaların gelişimine imkân sağlamaktır. Rotor dinamiğinin tahmin edilmesi birçok makina için önemli sonuçlara sahiptir. Dönen bileşenlere sahip birçok makina vardır; örneğin türbin, kompresör, pompa, takım tezgâhı, helikopter ve dişçi gırgırı rotorları. Bu sistemlerin dinamiği arzu edilen şekilde çalışmaları, kararlılık, verimlilik ve sağlık açısından oldukça önemlidir. Keza, tahrik frekanslarından birinin sistemin doğal frekanslarından birine çok yakın olması gibi, eğer doğal frekanslardan biri çalışma alanı içinde ise sistem rezonansa girebilir ve ortaya çıkan büyük genlikli titreşimler işlemin hassasiyet ve verimliliğinde kayba yol açıp rulmanlarda ve makinanın diğer elemanlarında hasara neden olabilir.

Rotor dinamiği analizinde iki ana yaklaşım vardır. Kullanımda olan rotorlar için sistem dinamiği modal analiz gibi deneysel yöntemlerle elde edilebilir. Bu hızlı bir yaklaşım olmasına karşın, hali hazırda bir deney düzeneğinin kurulu olması gereklidir. Ayrıca, takım tezgahı anamilindeki değişik takım ve takım tutucular için olduğu gibi, eğer rotora değişik bileşenler eklenirse ölçümler her kombinasyon için tekrarlanmalıdır ve bu da birçok ölçüm yapılmasına ve makinanın verimli zamanında kayba neden olur. Tasarım sırasında rotor dinamiğinin tahmin edilmesi de dinamik analiz gerektiren önemli bir durumdur. Tabi ki böyle bir durumda deneysel yaklaşım uygulanabilir bir metot değildir. Bunun yerine dinamiğin tahmin edilmesinde sonlu elemanlar analizi kullanılabilir. Bu birçok durum için geçerli çözüm olabilir. Bununla beraber modelin geliştirilmesi için sertlik ve sönüm gibi temas parametrelerinin bilinmesi gerekir. Ayrıca mümkün olan en küçük dönme ataletiyle en büyük dinamik rijitliği sağlayacak en uygun tasarım için birçok simülasyon gerçekleştirilmelidir. Bu genellikle çok zaman alır ve en uygun konfigürasyon hiçbir zaman elde edilemeyebilir.

Bu çalışmanın amacı makinanın tasarımı ve çalıştırılması esnasında kullanılmak üzere rotor-rulman sistemlerinin dinamik analizi için hızlı bir metot geliştirmektir. Bu metot değişik geometrik konfigürasyonlar için kritik bölgelerde sistemin frekans cevabı fonksiyonunu çok hızlı bir şekilde belirlemek amacıyla kullanılabilir ve bu sayede tasarım optimize edilebilir. Rulman önyüklemeleri gibi sistemin bazı dâhili parametrelerinin değerleri ve etkileri de bu metot kullanılarak belirlenebilir. Ayrıca, rotora yeni bileşenlerin eklenmesinin ardından sistemin dinamik cevabı yenilenebilir.

This thesis is dedicated to *my love Melike*

She is the half that makes me whole

She is my light when I am lost in the dark

She is the reason that my hope is still alive

This thesis is dedicated to *my sweat mom*

She is why her every smile renews the life within me

She is why I still feel that I am a piece of her soul

She is why I am nothing when she is sad

ACKNOWLEDGEMENTS

I would like to express my special thanks to Associate Prof. Dr. Erhan Budak for his continuous help and guidance throughout the duration of this study. I would also like to express my appreciation to Assistant Prof. Dr. Serhat Yeşilyurt for his useful discussions and help. I would also like to thank Mehmet Güler for his great effort during the manufacturing of the experimental set-up.

Special thanks are due to the graduate students in the Mechatronics Program for their nice chat and friendship. This work would not have been possible without their encouragement.

I'd like to thank also to my family for their confidence in me that enabled me to complete this work. I should also acknowledge to some of my relatives for their motivation while I was writing my thesis and they were lying on the beach.

Finally, very special thanks for my love Melike who never kept me alone always being at my side.

TABLE OF CONTENTS

LIST OF TABLES

LIST OF FIGURES

TABLE OF SYMBOLS

x, y, z	:	Spatial coordinates
u_y	:	Displacement in y
$\emptyset_z$	:	Rotation about z
M	:	Moment
F	:	Shear force
l, L	:	Length
d, D	:	Diameter
t	:	Time
ρ	:	Mass density
E	:	Modulus of elasticity
A	:	Cross sectional area
I	:	Area moment of inertia
f	:	External load per unit length
$\lambda, \beta_n, \alpha_n$	:	Dimensionless parameters
Y	:	Spatial part of y
A_1, B_1	:	Constants
T	:	Temporal part of y
w	:	Frequency
n	:	Mode number
w_n	:	Natural frequency
Y'	:	First derivative of Y with respect to x
H	:	Frequency response function
S, R	:	Deflection functions
C	:	Damping coefficient
ζ	:	Damping ratio
h	:	Hysteretic damping ratio
c_{eq}	:	Equivalent damping coefficient

A_n	:	Amplitude
$Ø_n$	:	Phase
r, R	:	Radius
Δ	:	Clearance
N	:	Applied radial force
δ	:	Deformation
p	:	Pressure
k	:	Linear contact compliance
c	:	Nonlinear contact compliance
v	:	Poisson's ratio
γ	:	Angle between the balls of the bearing
z	:	Number of balls
α	:	Contact angle of bearing
μ	:	Friction coefficient
P	:	Load
K	:	Stiffness
m	:	Mass per unit length
Hz	:	Hertz
MPa, GPa	:	MegaPascal, GigaPascal
$\mu m, mm$	:	Micrometer, Millimeter
κ	:	Timoshenko's shear coefficient
D_{11}	:	Deflection related FRF
S_{11}	:	Slope related FRF
θ	:	Slope

TABLE OF ABBREVIATIONS

CAD	**:**	Computer Aided Design
CNC	**:**	Computer Numerical Control
DOF	**:**	Degree of Freedom
E-B	**:**	Euler-Bernoulli
FEA	**:**	Finite Element Analysis
FEM	**:**	Finite Element Modelling
FFT	**:**	Fast Fourier Transform
FRF	**:**	Frequency Response Function
HSM	**:**	High Speed Machining
HSS	**:**	High Speed Spindle
3-D	**:**	3-Dimensional

RAPID MODELLING OF MULTI-STEPPED ROTOR DYNAMICS

by
HAKAN KESKİN

Submitted to the Graduate School of Engineering and Natural Sciences
in partial fulfillment of
the requirements for the degree of
Master of Science

SABANCI UNIVERSITY
Spring 2004

RAPID MODELLING OF MULTI-STEPPED ROTOR DYNAMICS

APPROVED BY:

Associate Prof. Dr. ERHAN BUDAK .....
(Dissertation Advisor)

Assistant Prof. Dr. SERHAT YEŞİLYURT .....
(Dissertation Co-Advisor)

Prof. Dr. ASIF ŞABANOVİÇ .....

Assistant Prof. Dr. KEMALETTİN ERBATUR .....

Assistant Prof. Dr. AYHAN BOZKURT .....

DATE OF APPROVAL: .....

ABSTRACT

The major objective of the studies on the dynamic behaviour of rotors is to allow development of rotating machinery that will be free from vibrational problems. Rotor dynamics prediction has several important consequences for a large group of machinery. First of all, there are many machines with rotating components, i.e. rotors, such as turbines, compressors and pumps, machine tools, helicopters, dentist's tooth grinders etc. The dynamics of these systems are very critical for their proper functioning, stability, efficiency and health. For example, if one of the natural frequencies is in the operation region of the system, i.e. one of the excitation frequencies during the operation is close to one of the natural frequencies, then the system may resonate and the resulting large amplitude vibrations will cause loss of accuracy and efficiency in the operation, and may also damage the bearings and the rest of the machinery.

There are two main approaches to rotor dynamics analysis. For existing rotors, the dynamics can be measured using experimental techniques such as modal analysis. Although this can be a fast approach, it requires the experimental set up be available. Also, if there are many different components added to the rotor, such as different tool holders and tools on a machine tool spindle, then the measurements must be repeated for each combination which may result in high number of tests and waste of productive time on the machine. Prediction of the rotor dynamics during the design is another critical case where dynamics analysis is required. Obviously, testing is not a possible technique for this case. FEA can be used for the prediction of the dynamics. This may be a viable solution in many cases, however the bearing contact parameters, i.e. stiffness and damping, must be known in order to develop the model. Also, many simulations have to be performed for optimal design resulting in highest dynamic rigidity with smallest possible rotary inertia. This is usually very time consuming, and the optimal configuration may never be obtained.

The objective of this study is to develop a fast method for the dynamic analysis of rotor-bearing systems so that they can be used during the design and the operation of the machinery. The method can be used to determine the frequency response function of the system at critical locations for different geometric configurations very fast so that the design could be optimized. The effects and optimal values of some internal system parameters such as bearing preloads could also be determined using the method. Also, the dynamic response of the system could be updated after new components are added to the rotor.

ÖZET

Rotorların dinamik davranışı üzerine yapılan çalışmaların ana amacı titreşim problemlerine maruz kalmayan dönen makinaların gelişimine imkân sağlamaktır. Rotor dinamiğinin tahmin edilmesi birçok makina için önemli sonuçlara sahiptir. Dönen bileşenlere sahip birçok makina vardır; örneğin türbin, kompresör, pompa, takım tezgâhı, helikopter ve dişçi gırgırı rotorları. Bu sistemlerin dinamiği arzu edilen şekilde çalışmaları, kararlılık, verimlilik ve sağlık açısından oldukça önemlidir. Keza, tahrik frekanslarından birinin sistemin doğal frekanslarından birine çok yakın olması gibi, eğer doğal frekanslardan biri çalışma alanı içinde ise sistem rezonansa girebilir ve ortaya çıkan büyük genlikli titreşimler işlemin hassasiyet ve verimliliğinde kayba yol açıp rulmanlarda ve makinanın diğer elemanlarında hasara neden olabilir.

Rotor dinamiği analizinde iki ana yaklaşım vardır. Kullanımda olan rotorlar için sistem dinamiği modal analiz gibi deneysel yöntemlerle elde edilebilir. Bu hızlı bir yaklaşım olmasına karşın, hali hazırda bir deney düzeneğinin kurulu olması gereklidir. Ayrıca, takım tezgahı anamilindeki değişik takım ve takım tutucular için olduğu gibi, eğer rotora değişik bileşenler eklenirse ölçümler her kombinasyon için tekrarlanmalıdır ve bu da birçok ölçüm yapılmasına ve makinanın verimli zamanında kayba neden olur. Tasarım sırasında rotor dinamiğinin tahmin edilmesi de dinamik analiz gerektiren önemli bir durumdur. Tabi ki böyle bir durumda deneysel yaklaşım uygulanabilir bir metot değildir. Bunun yerine dinamiğin tahmin edilmesinde sonlu elemanlar analizi kullanılabilir. Bu birçok durum için geçerli çözüm olabilir. Bununla beraber modelin geliştirilmesi için sertlik ve sönüm gibi temas parametrelerinin bilinmesi gerekir. Ayrıca mümkün olan en küçük dönme ataletiyle en büyük dinamik rijitliği sağlayacak en uygun tasarım için birçok simülasyon gerçekleştirilmelidir. Bu genellikle çok zaman alır ve en uygun konfigürasyon hiçbir zaman elde edilemeyebilir.

Bu çalışmanın amacı makinanın tasarımı ve çalıştırılması esnasında kullanılmak üzere rotor-rulman sistemlerinin dinamik analizi için hızlı bir metot geliştirmektir. Bu metot değişik geometrik konfigürasyonlar için kritik bölgelerde sistemin frekans cevabı fonksiyonunu çok hızlı bir şekilde belirlemek amacıyla kullanılabilir ve bu sayede tasarım optimize edilebilir. Rulman önyüklemeleri gibi sistemin bazı dâhili parametrelerinin değerleri ve etkileri de bu metot kullanılarak belirlenebilir. Ayrıca, rotora yeni bileşenlerin eklenmesinin ardından sistemin dinamik cevabı yenilenebilir.

This thesis is dedicated to *my love Melike*

She is the half that makes me whole

She is my light when I am lost in the dark

She is the reason that my hope is still alive

This thesis is dedicated to *my sweat mom*

She is why her every smile renews the life within me

She is why I still feel that I am a piece of her soul

She is why I am nothing when she is sad

ACKNOWLEDGEMENTS

I would like to express my special thanks to Associate Prof. Dr. Erhan Budak for his continuous help and guidance throughout the duration of this study. I would also like to express my appreciation to Assistant Prof. Dr. Serhat Yeşilyurt for his useful discussions and help. I would also like to thank Mehmet Güler for his great effort during the manufacturing of the experimental set-up.

Special thanks are due to the graduate students in the Mechatronics Program for their nice chat and friendship. This work would not have been possible without their encouragement.

I'd like to thank also to my family for their confidence in me that enabled me to complete this work. I should also acknowledge to some of my relatives for their motivation while I was writing my thesis and they were lying on the beach.

Finally, very special thanks for my love Melike who never kept me alone always being at my side.

TABLE OF CONTENTS

LIST OF TABLES

LIST OF FIGURES

TABLE OF SYMBOLS

x, y, z	:	Spatial coordinates
u_y	:	Displacement in y
$\emptyset_z$	:	Rotation about z
M	:	Moment
F	:	Shear force
l, L	:	Length
d, D	:	Diameter
t	:	Time
ρ	:	Mass density
E	:	Modulus of elasticity
A	:	Cross sectional area
I	:	Area moment of inertia
f	:	External load per unit length
$\lambda, \beta_n, \alpha_n$	:	Dimensionless parameters
Y	:	Spatial part of y
A_1, B_1	:	Constants
T	:	Temporal part of y
w	:	Frequency
n	:	Mode number
w_n	:	Natural frequency
Y'	:	First derivative of Y with respect to x
H	:	Frequency response function
S, R	:	Deflection functions
C	:	Damping coefficient
ζ	:	Damping ratio
h	:	Hysteretic damping ratio
c_{eq}	:	Equivalent damping coefficient

A_n	:	Amplitude
$Ø_n$	:	Phase
r, R	:	Radius
Δ	:	Clearance
N	:	Applied radial force
δ	:	Deformation
p	:	Pressure
k	:	Linear contact compliance
c	:	Nonlinear contact compliance
v	:	Poisson's ratio
γ	:	Angle between the balls of the bearing
z	:	Number of balls
α	:	Contact angle of bearing
μ	:	Friction coefficient
P	:	Load
K	:	Stiffness
m	:	Mass per unit length
Hz	:	Hertz
MPa, GPa	:	MegaPascal, GigaPascal
$\mu m, mm$	:	Micrometer, Millimeter
κ	:	Timoshenko's shear coefficient
D_{11}	:	Deflection related FRF
S_{11}	:	Slope related FRF
θ	:	Slope

TABLE OF ABBREVIATIONS

CAD	**:**	Computer Aided Design
CNC	**:**	Computer Numerical Control
DOF	**:**	Degree of Freedom
E-B	**:**	Euler-Bernoulli
FEA	**:**	Finite Element Analysis
FEM	**:**	Finite Element Modelling
FFT	**:**	Fast Fourier Transform
FRF	**:**	Frequency Response Function
HSM	**:**	High Speed Machining
HSS	**:**	High Speed Spindle
3-D	**:**	3-Dimensional

1 INTRODUCTION

The major objective of the studies on the dynamic behaviour of rotors is to allow development of rotating machinery that will be free from vibrational problems. A rotor is a body suspended through a set of cylindrical supports, e.g. bearings, that allow it to rotate freely about an axis fixed in space. Transmission shafts, parts of reciprocating machines that have only rotational motion and many other rotating machine elements can thus be considered as rotors. An example of a rotor-bearing system with three bearings can be seen in Figure 1.1.

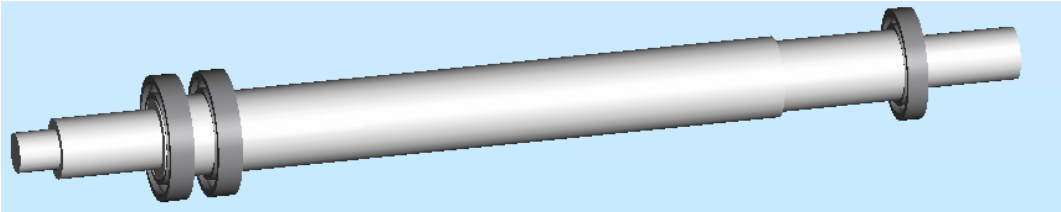

Figure 1.1: Rotor-bearing system.

A rotor has a well defined and fixed rotation axis if it is perfectly balanced. Actually, this is only approximately true, but the unbalance is usually small. Another common assumption is that of axial symmetry of the rotor.

In earlier studies it was seen that the fundamental frequency for torsional deformation of slender bar is much higher than it is for flexure [1]. We therefore focus on flexure, and consider the shaft to be rigid in torsion. Flexural vibration of a rotor is the vibration in the direction perpendicular to its length. One can also assume that the flexural natural frequencies are independent of the speed and the forcing frequencies.

Thus, for the study of the flexural vibration, rotor can be assumed as a circular beam with multiple segments. Most common models for flexural vibration of beams are *Euler-Bernoulli* and *Timoshenko* beam models both of which have specific assumptions since it is quite difficult to construct a single model that describes all effects.

Elasticity effect associated with the bearings which are considered to be rigid in the beam models can be extremely important. Forces exerted by the bearings on the shaft require reactions that are applied to the supporting structure, thereby causing displacement. Stiffness coefficients describe the relation between the displacement and the forces.

Another source of elasticity lies within the bearings themselves. Ball and roller bearings have some elastic features that are unrelated to the behaviour of the supporting structure.

Also the energy dissipation has significant effects on the system dealt. An obvious source of dissipation is external damping resulting from the interactions of the shaft, bearings and housings. Another source of dissipation is internal damping, which can arise from internal inelastic effects.

The influence of damping parameters of the supporting elements of the rotor is more difficult to assess than its stiffness. It depends not only on parameters (stiffness and damping) of the supporting elements, but also on rather complex relations between dynamic characteristics of the rotor and the supporting system. For the reason of this complexity, equivalent damping of the system has to be estimated by experimental methods.

A comprehensive study of rotor dynamics is multidisciplinary since the dynamic behaviour depends also on the behaviour of the bearings and their housings apart from the rotor. In some modern engineering applications, such as high speed gas turbines, machine tool spindles, and gyroscopes, the bearings are often must be treated as an integral to the system to be able to accurately determine shaft deflections and dynamic shaft loading.

The spin speeds at which one of the forcing functions has a frequency coinciding with one of the flexural natural frequencies of the system are usually referred as critical speeds. If the frequency of a forcing function coincides with natural frequency of a mode, resonance occurs. In case of the system damping is not sufficient, a very strong resonance may take place and the rotor cannot operate at or near a critical speed without having strong vibrations and even a catastrophic failure.

When a rotor operates at a critical speed, the amplitude of the vibration grows in time and only the damping of the system can prevent the failure of the rotor. The resonance frequency can be shifted by a proper choice of stiffness and mass values and distribution. While shifting of the resonance frequencies may help to avoid the

excessive resonance displacement amplitudes and overloads, this can help only if the forcing frequencies are determined and do not vary significantly. In many cases this is not a realistic assumption. For example, the forcing frequencies acting on a machine tool during milling operation change with the number of cutting inserts in the milling cutter and with the spindle speed.

High speed spindles are the most critical elements of the high speed machining systems, which has become a hot area of development due to many benefits it provides. High Speed Machining is any CNC milling machine process that utilizes faster spindle rates, feed rates, and better tooling technology for higher production rates than a conventional or previously developed machining process.

The technology of HSM is still relatively new. Because of the lack of experience in this new field, there are still many problems to be solved in the application of HSM, including the dynamic behaviours of the spindle. An example of a high speed spindle can be seen in Figure 1.2 in detail.

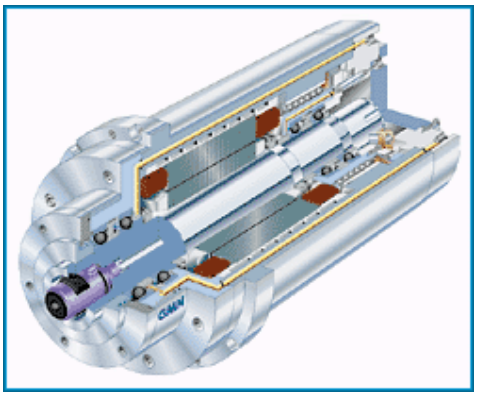

Figure 1.2: GMN-Model HSP high frequency spindle [2].

One of the most critical components of any high speed spindle is the bearing system. Angular contact bearings are most commonly used today in very high speed spindle designs. This is due to the fact that angular contact ball bearings provide the precision, load carrying capacity and speed required for metal cutting spindles. In some cases, tapered roller bearings are used, due to their higher load capacity and greater stiffness over ball bearings. However, tapered roller bearings do not allow the high speeds required by many spindles.

Angular contact ball bearings are manufactured to a specification that includes a contact angle. The contact angle is the nominal angle between the ball-to-race contact line and a plane through the ball centres, perpendicular to the bearing axis.

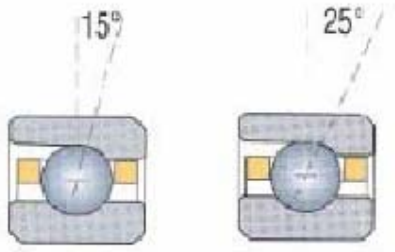

Figure 1.3: Contact angle of angular contact ball bearings.

The contact angle determines the ratio of axial to radial loading possible, with radial loading being the primary benefit. Typical contact angles are 15º and 25º as shown in Figure 1.3. The lower the contact angle, the greater the radial load carrying capacity, the higher the contact angle the higher the axial loading capacity will be.

Angular contact ball bearings are available with a choice of pre-loading magnitude, typically designated as light, medium and heavy.

1.1 Related Literature Review

Compared to the bibliography on the transverse vibration of single span Euler-Bernoulli beams, publications on beams with step changes is not extensive. Jang and Bert [3,4] were the first to derive the frequency equations of beams with one step change in cross-section as fourth order determinants equated to zero, for the combinations of classical boundary conditions. Nagulesvaran [5] proposed a method to calculate the first three frequencies of beams up to three step changes in cross-section. Because of the computational difficulties number of natural frequencies that can be obtained is highly dependent on the complexity of the beam (number of segments, length/diameter ratios, etc…).

Many researchers have investigated the dynamic aspects of spindles. Many simulation methods based on the system dynamics have been developed to establish a model prediction for the mechanical and thermal behaviour of a spindle-bearing system. Li and Shin [6,7] developed a computer program to generate comprehensive solutions for high speed spindle-bearing systems based on an integrated thermo-mechanical spindle model presented. Spiweak and Nickel [8] proposed an algorithm for the

prevention of catastrophic bearing failures caused by excessive thermally induced preload.

In a high-speed spindle system, the bearing characteristics are influenced significantly by the initial assembly tolerances and the thermal deformation of the bearing surroundings. Kim, K.Lee and J.Lee [9,10] considered the bearing surroundings such as assembly tolerance, geometric dimension, cooling conditions, operating conditions and thermal deformation.

Shaft and bearing systems form the hearth of many machines and mechanisms such as machine tool spindles, engines and turbo-machinery. Bearings often represent the limiting factor in machines' performance under dynamic conditions. L.Ynagh, Rahnejat and Aini [11] presented a detailed model of bearing vibration, including the effect of contact spring nonlinearity in balls-to raceways contacts. . Aktürk and Gohar [12] investigated the effect of ball size variation in the bearings on the vibration of the shaft. And Li and Shin [13] presented the effects of bearing configuration on the behaviour of high speed spindles. Finally Lin, Tu and Kamman [14] investigates the bearing preload effects on bearing stiffness, and subsequently on overall spindle dynamics

The finite element method has been established as the major tool for the dynamic analysis of engineering structures. However, an alternative approach, where a complex structure may be divided into smaller components, is still necessary because of practical considerations.

For the estimation of the frequency response functions of rotor-bearing systems and its individual components, modal analysis is widely used in recent years by means of experimental measurement of the response data. Peeters, Pintelon, Schoukens and Rolain [15,16] estimated the frequency response functions of the rotor-bearing systems on the basis of the maximum likelihood estimator, considering noise on both inputs and outputs of experimental data. They also discussed the parametric identification of the system in frequency domain, which is developed for real as well as for complex modal testing.

Several coupling algorithms are well established for combining the characteristics (frequency response functions) of the substructures of the rotor-bearing systems. Choi and Park [17] presented the application of impedance coupling method and the equivalent rotor model for including the support dynamics on the interaction with the rotor. Chong and Imregun [18] discussed a general methodology for the coupling

analysis of systems with relative weak non-linearities by assuming that the response remains harmonic under harmonic excitation. And Ewins developed a general FRF coupling analysis with and without including the joint parameters in [19] and in his book [20].

1.2 Scope of the Study

Rotor dynamics prediction has several important consequences for a large group of machinery. First of all, there are many machines with rotating components, i.e. rotors, such as turbines, compressors and pumps, machine tools, helicopters, dentist's tooth grinders etc… The dynamics of these systems are very critical for their proper functioning, stability, efficiency and health. For example, if one of the natural frequencies is in the operation region of the system, i.e. one of the excitation frequencies during the operation is close to one of the natural frequencies, then the system may resonate and the resulting large amplitude vibrations will cause loss of accuracy and efficiency in the operation, and may also damage the bearings and the rest of the machinery. In case of a helicopter, the ride comfort will be compromised, and the flight safety will be threatened. In case of a machining centre, the chatter vibrations will limit the productivity and result in poor surface finish. In almost all of these applications, the rotor is the weakest part of the machine as it is usually supported at a limited number of points by bearings. In addition, the diameter of the rotor is kept as small as possible, especially for high speed machines, in order to reduce the rotational inertia so that the rotational acceleration is increased, and the maximum speeds can be reached faster. The maximum temperature that can be tolerated by the roller bearings indicated by the DN (diameter times the maximum rpm) number also imposes limitations on the rotor diameter.

There are two main approaches to rotor dynamics analysis. For existing rotors, the dynamics can be measured using experimental techniques such as modal analysis. Although this can be a fast approach, it requires the experimental set up be available. Also, if there are many different components added to the rotor, such as different tool holders and tools on a machine tool spindle, then the measurements must be repeated for each combination which may result in high number of tests and waste of productive

time on the machine. Prediction of the rotor dynamics during the design is another critical case where dynamics analysis is required. Obviously, testing is not a possible technique for this case. FEA can be used for the prediction of the dynamics. This may be a viable solution in many cases, however the bearing contact parameters, i.e. stiffness and damping, must be known in order to develop the model. Also, many simulations have to be performed for optimal design resulting in highest dynamic rigidity with smallest possible rotary inertia. This is usually very time consuming, and the optimal configuration may never be obtained.

The objective of this study is to develop a fast method for the dynamic analysis of rotor-bearing systems so that they can be used during the design and the operation of the machinery. The method can be used to determine the frequency response function of the system at critical locations for different geometric configurations very fast so that the design could be optimized. The effects and optimal values of some internal system parameters such as bearing preloads could also be determined using the method. Also, the dynamic response of the system could be updated after new components are added to the rotor.

In Chapter 2 a method for dynamic modelling of multi-stepped beams is proposed. The method mainly depends on the coupling of segments modelled with Euler-Bernoulli beam model and is capable of calculating the natural frequencies and mode shapes. Also, a formulation of the forced vibration for multi-stepped beams to obtain the frequency response function corresponding to any point on the beam is developed for both undamped and damped cases.

Chapter 3 discusses the contact stiffness between the shaft and the bearing. A model for nonlinear stiffness estimations is developed for the cylindrical connections with clearance fit and ball bearings. Finally, preload force equilibrium formulation of the rotor-bearing systems is presented.

In Chapter 4 analytical models discussed in Chapter 2 and 3 are implemented, and some the results are compared with finite element modelling. First, results of two models for a simple beam are compared. Then, the analysis is performed starting from free-free multi-stepped beam and ending with the rotor-bearing system. For all of the steps, natural frequencies, mode shapes and frequency response functions are compared and discussed. Determination of the friction coefficient between outer races of the bearings and the housings also explained in detail.

Chapter 5 first presents the specifications of the experimental set-up, then explains the methods used in the experiments. Some of the results are compared with the analytical models. For the determination of the connection parameters between the rotor and the housing, the receptance coupling method is applied. Results are compared with the analytically obtained stiffness values and discussed.

A conclusion of the work is provided in Chapter 6 summarizing the results obtained and achievements.

2 TRANSVERSE VIBRATION OF MULTI-STEPPED BEAMS

This chapter considers the vibration of multi-stepped beams in the direction perpendicular to its length. Such vibrations are called *transverse* or *flexural vibration* since they move across the length of the beam.

An elastic beam possesses both the mass and stiffness to resist bending. During transverse vibration, the beam flexes perpendicular to its own axis to alternately store potential energy in the elastic bending of the beam and then release it into kinetic energy of transverse motion.

In bending two of the degrees of freedom of each cross section is involved. If bending occurs in $x-y$ plane, the relevant degrees of freedoms are displacement u_y and rotation ϕ_z.

2.1 Euler-Bernoulli Beam

The simplest approach for the study of flexural behaviour of the beam is that often defined as Euler-Bernoulli beam, based on the added assumptions that both shear deformation and rotational inertia of the cross sections are negligible compared with bending deformation and translational inertia, respectively. This assumption leads to a good approximation if the beam is very slender, i.e., if the thickness in the y-direction is much smaller than length *l (l/d >10).*

The other important assumptions used in formulating Euler-Bernoulli beam model are that the beam is

- Uniform along its span
- Composed of a linear, homogeneous, isotropic elastic material without axial loads
- Such that plane sections remain plane

- Such that the plane of symmetry of the beam is also the plane of vibration so that rotation and translation are decoupled.

Consider a uniform beam made of a material of mass density ρ and modulus of elasticity E, cross sectional area A, and area moment of inertia I. Let x be a coordinate along the neutral axis of the beam, measured from its left end. The beam has an external load per unit length, $f(x,t)$. Let $y(x,t)$ be transverse deflection of the beam, measured from its equilibrium position.

Free body diagram of an arbitrary differential element of the beam at an arbitrary instant of time is shown in Figure 2.1. The element is a slice of the beam of thickness dx and its centre is a distance x from the left end of the beam.

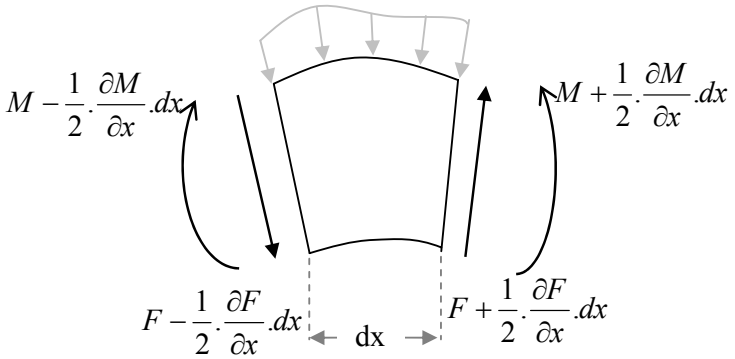

Figure 2.1: Forces and moments acting on the length of the beam.

Summing the forces in the vertical direction and moments about the neutral axis at the centre of the element, and neglecting the terms of order dx^2 since dx is infinitesimal leads to [21]

$$A(x).\rho(x).\frac{\partial^2 y(x,t)}{\partial t^2} + \frac{\partial^2}{\partial x^2}\left(E(x).I(x).\frac{\partial^2 y(x,t)}{\partial x^2}\right) = f(x,t) \tag{2.1}$$

If the beam is uniform (the parameters A, I, E and ρ are constant) motion of the beam is governed by the following equation

$$\frac{\partial^2 y(x,t)}{\partial t^2} + \lambda^2.\frac{\partial^4 y(x,t)}{\partial x^4} = q(x,t) \tag{2.2}$$

where

$$\lambda^2 = \frac{E.I}{A.\rho} \quad \text{and} \quad q(x,t) = \frac{f(x,t)}{A.\rho} \tag{2.3}$$

2.2 Free Vibration of Beams

2.2.1 Single Span Uniform Beams

Equation (2.2) can be classified as linear partial differential equation of two variables (x and t) with constant coefficients (λ^2) with the order of 2 with respect to time and 4 with respect to x. If the external excitation $q(x,t)=0$, this equation describes the free vibration of the beam due to non-zero initial conditions.

$$\frac{\partial^2 y(x,t)}{\partial t^2}+\lambda^2.\frac{\partial^4 y(x,t)}{\partial x^4}=0 \tag{2.4}$$

Using the method of separation of variables predicted solution is

$$y(x,t)=Y(x).T(t) \tag{2.5}$$

Substituting Equation (2.5) into Equation (2.4) the result is

$$-\frac{1}{T(t)}.\frac{d^2T(t)}{dt^2}=\frac{\lambda^2}{Y(x)}.\frac{d^4Y(x)}{dx^4}=C \tag{2.6}$$

When the first and third part equality is considered

$$\frac{d^2T(t)}{dt^2}+C.T(t)=0 \tag{2.7}$$

It is obvious that $C=w_n{}^2$ and the solution corresponding to the nth mode is as in the case of an undamped single degree of freedom system

$$T_n(t)=A_n.\cos(w_nt)+B_n.\sin(w_nt) \tag{2.8}$$

where the constants A_n and B_n will eventually be determined by the initial conditions after being combined with the spatial solution.

The spatial equation comes from rearranging Equation (2.6), which yields

$$\frac{d^4Y_n(x)}{dx^4}-\beta_n{}^4.Y_n(x)=0 \tag{2.9}$$

where

$$\beta_n{}^4=\frac{\mathrm{w_n}^2}{\lambda^2}=\frac{A.\rho.w_n{}^2}{E.I} \tag{2.10}$$

The standard form of this particular solution is

$$Y_n(x) = e^{r.x} \tag{2.11}$$

with

$$r^4 = \beta_n{}^4 \text{ and its roots } r_1 = \beta_n,\ r_2 = -\beta_n,\ r_3 = i.\beta_n,\ r_4 = -i.\beta_n \tag{2.12}$$

this brings the general solution of Equation (2.9) as [22]

$$Y_n(x) = A_{1n}.\sinh(\beta_n.x) + A_{2n}.\cosh(\beta_n.x) + A_{3n}.\sin(\beta_n.x) + A_{4n}.\cos(\beta_n.x) \tag{2.13}$$

Here the value for β_n and three of the constants A_{1n}, A_{2n}, A_{3n} and A_{4n} can be determined from the four boundary conditions. The fourth constant becomes combined with the constants A_n and B_n of the Equation (2.8), which are then determined from the initial conditions.

For a uniform single span beam, four boundary conditions are needed and two equations must be written for each end. For a free end the bending moment and shear force, for a clamped (or fixed) end the deflection and slope, for a pinned end the deflection and bending moment, and for a sliding end the slope and shear force must vanish and that's why they should be zero. For an end with spring and damper the bending moment vanishes but the shear force is balanced with the spring and the damper forces.

The slope, bending moment and shear force equations of the boundaries are directly proportional with the first, second and third derivatives of $Y_n(x)$ with respect to x, respectively, which are

$$\begin{aligned}
&Y_n{}^{I}(x) = A_{1n}.\beta_n.\cosh(\beta_n.x) + A_{2n}.\beta_n.\sinh(\beta_n.x) + \\
&A_{3n}.\beta_n.\cos(\beta_n.x) - A_{4n}.\beta_n.\sin(\beta_n.x) \\
&Y_n{}^{II}(x) = A_{1n}.\beta_n{}^2.\sinh(\beta_n.x) + A_{2n}.\beta_n{}^2.\cosh(\beta_n.x) - \\
&A_{3n}.\beta_n{}^2.\sin(\beta_n.x) - A_{4n}.\beta_n{}^2.\cos(\beta_n.x) \\
&Y_n{}^{III}(x) = A_{1n}.\beta_n{}^3.\cosh(\beta_n.x) + A_{2n}.\beta_n{}^3.\sinh(\beta_n.x) - \\
&A_{3n}.\beta_n{}^3.\cos(\beta_n.x) + A_{4n}.\beta_n{}^3.\sin(\beta_n.x)
\end{aligned} \tag{2.14}$$

$Y_n{}^{I}(x)$ stands for the first derivative of $Y_n(x)$ with respect to x and so on for the others. Applying these equations for the boundary conditions of the beam mode shape corresponding to any nth natural frequencies can easily be determined.

Moreover, Equation (2.10) allows the natural frequencies to be computed:

$$w_n = \beta_n{}^2 . \sqrt{\frac{E.I}{A.\rho}} \tag{2.15}$$

2.2.2 Multi-Stepped Beams

Compared to the studies done on the transverse vibration of uniform single span Euler-Bernoulli beams, studies on beams with step changes in cross section is not extensive. In this section multi-stepped beams are considered as combinations of uniform beams by means of continuity equations.

When the whole beam is considered, due to step changes in cross section Equation (2.1) cannot take the form of Equation (2.2). For this reason, to obtain the natural frequencies and mode shapes of the beam by application of the procedure described in section 1.2.1 to the whole beam is not possible. Instead, every span should be dealt with their own mode shapes according to their boundary conditions.

In the case of multi-stepped beams some of the equations related to boundary conditions are obtained from continuity equations. For a step change in cross section continuity conditions of the deflection, slope, bending moment and shear force result in four boundary equations that are needed for two coupled beam spans. One important remark here is that the area moment of inertias must be taken into consideration in the equivalence of the bending moments and shear forces of the coupled spans.

A span with a pin or spring support in the mid is considered as two separate spans. For the case of the pin support, four boundary conditions result from the continuity conditions of the slopes and bending moments, and the elimination of the deflections of the ends of the coupled spans. On the other hand, for the spring supported span in the middle, four boundary conditions result from the continuity conditions of the deflections, slopes and bending moments, along with the equivalence of the shear force difference between the ends of the spans to the spring force.

A slender beam with n step changes in cross section and m supports in the middle has a total number of spans of (n+m+1), n+1 from step changes and m from supports. All these spans should be treated separately, and then be coupled to obtain the natural frequencies and mode shapes of the whole beam. This yields that for a slender beam with N spans, there should be N spatial equations (Equation (2.13)), which results in

$5N$ unknowns (β and four constants). However there are only N spans, and 4 N boundary or continuity equations which are not enough to determine $5N$ unknowns.

The solution comes from the natural frequency of the beam. Since the natural frequencies of the beam apply for the all spans, β values for all spans can be written in terms of β of one of the spans. So, the number of unknowns diminishes to 4N+1 which is one more than the number of equations as in the case of single span beams.

For an illustration of the described method, consider the beam in Figure 2.2 with two segments of different cross sections. Since there is no support in the middle of the beam and there is only one step change in cross section, it is a two-span beam.

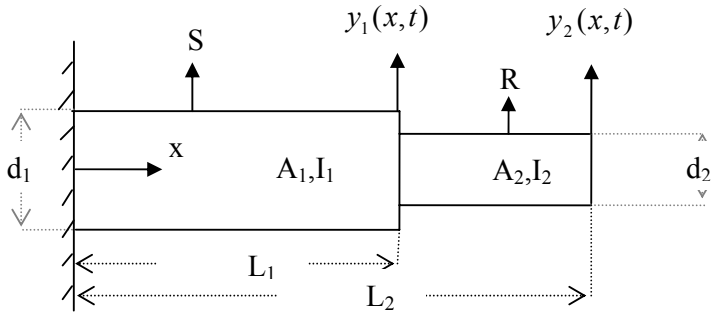

Figure 2.2: A two-span beam with one step change in cross section.

Applying of Equation (2.9) for the two spans

$$\frac{d^4 S_n(x)}{dx^4} - \alpha_n{}^4 . S_n(x) = 0 \quad , \quad 0 \le x \le L_1$$
$$\frac{d^4 R_n(x)}{dx^4} - \beta_n{}^4 . R_n(x) = 0 \quad , \quad L_1 \le x \le L_2 \tag{2.16}$$

where

$$\alpha_n = \beta_n . \sqrt{\frac{d_2}{d_1}} \tag{2.17}$$

since

$$w_n = \beta_n{}^2 . \sqrt{\frac{E.I_2}{A_2 . \rho}} = \alpha_n{}^2 . \sqrt{\frac{E.I_1}{A_1 . \rho}} \tag{2.18}$$

The solution for Equation (2.16) is

$$R_n(x) = A_{1n}.\sinh(\beta_n.x) + A_{2n}.\cosh(\beta_n.x) + A_{3n}.\sin(\beta_n.x) + A_{4n}.\cos(\beta_n.x)$$
$$S_n(x) = A_{5n}.\sinh(\alpha_n.x) + A_{6n}.\cosh(\alpha_n.x) + A_{7n}.\sin(\alpha_n.x) + A_{8n}.\cos(\alpha_n.x) \quad (2.19)$$

where A_{1n}, $A_{2n}, A_{3n}, A_{4n}, A_{5n}, A_{6n}, A_{7n}$ and A_{8n} are arbitrary constants. It is necessary to accompany the general solutions with boundary conditions. The boundary conditions are as follows.

At $x = L_2$ (i.e. at the free end), bending moment and shear force must vanish:

$$E.I_2.\frac{d^2R(L_2)}{dx^2} = 0 \rightarrow \frac{d^2R(L_2)}{dx^2} = 0 \quad (2.20)$$
$$A_{1n}.\sinh(\beta_n.L_2) + A_{2n}.\cosh(\beta_n.L_2) - A_{3n}.\sin(\beta_n.L_2) - A_{4n}.\cos(\beta_n.L_2) = 0$$

and

$$E.I_2.\frac{d^3R(L_2)}{dx^3} = 0 \rightarrow \frac{d^3R(L_2)}{dx^3} = 0 \quad (2.21)$$
$$A_{1n}.\cosh(\beta_n.L_2) + A_{2n}.\sinh(\beta_n.L_2) - A_{3n}.\cos(\beta_n.L_2) + A_{4n}.\sin(\beta_n.L_2) = 0$$

At $x = L_1$ the continuity equations for displacement, slope, bending moment and shear force are as follows:

$$R(L_1) = S(L_1)$$
$$A_{1n}.\sinh(\beta_n.L_1) + A_{2n}.\cosh(\beta_n.L_1) + A_{3n}.\sin(\beta_n.L_1) + A_{4n}.\cos(\beta_n.L_1) - A_{5n}.\sinh(\alpha_n.L_1) - A_6.\cosh(\alpha_n.L_1) - A_{7n}.\sin(\alpha_n.L_1) - A_{8n}.\cos(\alpha_n.L_1) = 0 \quad (2.22)$$

$$\frac{dR(L_1)}{dx} = \frac{dS(L_1)}{dx}$$
$$A_{1n}.\cosh(\beta_n.L_1) + A_{2n}.\sinh(\beta_n.L_1) + A_{3n}.\cos(\beta_n.L_1) - A_{4n}.\sin(\beta_n.L_1) - \frac{\alpha_n}{\beta_n}.A_{5n}.\cosh(\alpha_n.L_1) - \frac{\alpha_n}{\beta_n}.A_6.\sinh(\alpha_n.L_1) - \frac{\alpha_n}{\beta_n}.A_{7n}.\cos(\alpha_n.L_1) + \frac{\alpha_n}{\beta_n}.A_{8n}.\sin(\alpha_n.L_1) = 0 \quad (2.23)$$

$$\frac{d^2R(L_1)}{dx^2} = \frac{d^2S(L_1)}{dx^2}$$

$$\begin{aligned} &A_{1n}.\sinh(\beta_n.L_1) + A_{2n}.\cosh(\beta_n.L_1) - A_{3n}.\sin(\beta_n.L_1) - A_{4n}.\cos(\beta_n.L_1) - \\ &\left(\frac{\alpha_n}{\beta_n}\right)^2.A_{5n}.\sinh(\alpha_n.L_1) - \left(\frac{\alpha_n}{\beta_n}\right)^2.A_6.\cosh(\alpha_n.L_1) + \\ &\left(\frac{\alpha_n}{\beta_n}\right)^2.A_{7n}.\sin(\alpha_n.L_1) + \left(\frac{\alpha_n}{\beta_n}\right)^2.A_{8n}.\cos(\alpha_n.L_1) = 0 \end{aligned} \tag{2.24}$$

and

$$\frac{d^3R(L_1)}{dx^3} = \frac{d^3S(L_1)}{dx^3}$$

$$\begin{aligned} &A_{1n}.\cosh(\beta_n.L_1) + A_{2n}.\sinh(\beta_n.L_1) - A_{3n}.\cos(\beta_n.L_1) + A_{4n}.\sin(\beta_n.L_1) - \\ &\left(\frac{\alpha_n}{\beta_n}\right)^3.A_{5n}.\cosh(\alpha_n.L_1) - \left(\frac{\alpha_n}{\beta_n}\right)^3.A_6.\sinh(\alpha_n.L_1) + \\ &\left(\frac{\alpha_n}{\beta_n}\right)^3.A_{7n}.\cos(\alpha_n.L_1) - \left(\frac{\alpha_n}{\beta_n}\right)^3.A_{8n}.\sin(\alpha_n.L_1) = 0 \end{aligned} \tag{2.25}$$

At $x = 0$ (i.e. at the fixed end) displacement and slope are zero:

$$\begin{aligned} S(0) &= 0 \\ A_{6n} + A_{8n} &= 0 \end{aligned} \tag{2.26}$$

and

$$\begin{aligned} \frac{dS(0)}{dx} &= 0 \\ A_{5n} + A_{7n} &= 0 \end{aligned} \tag{2.27}$$

The Equations (2.20 – 2.27) result in a set of algebraic equations that are linear with respect to the constants A_{1n}, $A_{2n}, A_{3n}, A_{4n}, A_{5n}, A_{6n}, A_{7n}$ and A_{8n}. These equations can be written in the following form

$$D_n.A_n = 0 \tag{2.28}$$

where A_n is the vector of the constants with the dimension of (8 x 1), and D_n is the coefficient matrix of dimension (8 x 8) and is as it follows

$$D_n = \begin{bmatrix} \sinh(\beta_n.L_2) & \cosh(\beta_n.L_2) & -\sin(\beta_n.L_2) & -\cos(\beta_n.L_2) \\ \cosh(\beta_n.L_2) & \sinh(\beta_n.L_2) & -\cos(\beta_n.L_2) & \sin(\beta_n.L_2) \\ \sinh(\beta_n.L_1) & \cosh(\beta_n.L_1) & \sin(\beta_n.L_1) & \cos(\beta_n.L_1) \\ \cosh(\beta_n.L_1) & \sinh(\beta_n.L_1) & \cos(\beta_n.L_1) & -\sin(\beta_n.L_1) \\ \sinh(\beta_n.L_1) & \cosh(\beta_n.L_1) & -\sin(\beta_n.L_1) & -\cos(\beta_n.L_1) \\ \cosh(\beta_n.L_1) & \sinh(\beta_n.L_1) & -\cos(\beta_n.L_1) & \sin(\beta_n.L_1) \\ 0 & 0 & 0 & 0 \\ 0 & 0 & 0 & 0 \end{bmatrix} \cdots\cdots$$

$$\begin{bmatrix} 0 & 0 & 0 & 0 \\ 0 & 0 & 0 & 0 \\ -\sinh(\alpha_n.L_1) & -\cosh(\alpha_n.L_1) & -\sin(\alpha_n.L_1) & -\cos(\alpha_n.L_1) \\ -\frac{\alpha_n}{\beta_n}.\cosh(\alpha_n.L_1) & -\frac{\alpha_n}{\beta_n}.\sinh(\alpha_n.L_1) & -\frac{\alpha_n}{\beta_n}.\cos(\alpha_n.L_1) & \frac{\alpha_n}{\beta_n}.\sin(\alpha_n.L_1) \\ \cdots\cdots \left(\frac{\alpha_n}{\beta_n}\right)^2.\sinh(\alpha_n.L_1) & -\left(\frac{\alpha_n}{\beta_n}\right)^2.\cosh(\alpha_n.L_1) & \left(\frac{\alpha_n}{\beta_n}\right)^2.\sin(\alpha_n.L_1) & \left(\frac{\alpha_n}{\beta_n}\right)^2.\cos(\alpha_n.L_1) \\ -\left(\frac{\alpha_n}{\beta_n}\right)^3.\cosh(\alpha_n.L_1) & -\left(\frac{\alpha_n}{\beta_n}\right)^3.\sinh(\alpha_n.L_1) & \left(\frac{\alpha_n}{\beta_n}\right)^3.\cos(\alpha_n.L_1) & -\left(\frac{\alpha_n}{\beta_n}\right)^3.\sin(\alpha_n.L_1) \\ 0 & 1 & 0 & 1 \\ 1 & 0 & 1 & 0 \end{bmatrix}$$

(2.29)

The Equation (2.28) has a non-zero solution if and only if its characteristic determinant is equal to zero. This condition forms the so called characteristic equation

$$\begin{vmatrix} \sinh(\beta_n.L_2) & \cosh(\beta_n.L_2) & -\sin(\beta_n.L_2) & -\cos(\beta_n.L_2) \\ \cosh(\beta_n.L_2) & \sinh(\beta_n.L_2) & -\cos(\beta_n.L_2) & \sin(\beta_n.L_2) \\ \sinh(\beta_n.L_1) & \cosh(\beta_n.L_1) & \sin(\beta_n.L_1) & \cos(\beta_n.L_1) \\ \cosh(\beta_n.L_1) & \sinh(\beta_n.L_1) & \cos(\beta_n.L_1) & -\sin(\beta_n.L_1) \\ \sinh(\beta_n.L_1) & \cosh(\beta_n.L_1) & -\sin(\beta_n.L_1) & -\cos(\beta_n.L_1) \\ \cosh(\beta_n.L_1) & \sinh(\beta_n.L_1) & -\cos(\beta_n.L_1) & \sin(\beta_n.L_1) \\ 0 & 0 & 0 & 0 \\ 0 & 0 & 0 & 0 \end{vmatrix} \cdots\cdots$$

$$\begin{vmatrix} 0 & 0 & 0 & 0 \\ 0 & 0 & 0 & 0 \\ -\sinh(\alpha_n.L_1) & -\cosh(\alpha_n.L_1) & -\sin(\alpha_n.L_1) & -\cos(\alpha_n.L_1) \\ -\frac{\alpha_n}{\beta_n}.\cosh(\alpha_n.L_1) & -\frac{\alpha_n}{\beta_n}.\sinh(\alpha_n.L_1) & -\frac{\alpha_n}{\beta_n}.\cos(\alpha_n.L_1) & \frac{\alpha_n}{\beta_n}.\sin(\alpha_n.L_1) \\ \left(\frac{\alpha_n}{\beta_n}\right)^2.\sinh(\alpha_n.L_1) & -\left(\frac{\alpha_n}{\beta_n}\right)^2.\cosh(\alpha_n.L_1) & \left(\frac{\alpha_n}{\beta_n}\right)^2.\sin(\alpha_n.L_1) & \left(\frac{\alpha_n}{\beta_n}\right)^2.\cos(\alpha_n.L_1) \\ -\left(\frac{\alpha_n}{\beta_n}\right)^3.\cosh(\alpha_n.L_1) & -\left(\frac{\alpha_n}{\beta_n}\right)^3.\sinh(\alpha_n.L_1) & \left(\frac{\alpha_n}{\beta_n}\right)^3.\cos(\alpha_n.L_1) & -\left(\frac{\alpha_n}{\beta_n}\right)^3.\sin(\alpha_n.L_1) \\ 0 & 1 & 0 & 1 \\ 1 & 0 & 1 & 0 \end{vmatrix} = 0$$

(2.30)

Since the geometric dimensions L_1, L_2, d_1 and d_2 are known and α_n can be written in terms of β_n, the characteristic equation takes the form of a function of β_n. This function has infinite number of roots for the reason that the system dealt is a continuous system. From the corresponding roots of β_n natural frequencies of the beam can be obtained from Equation (2.18).

In order to obtain the mode shape of the beam corresponding to the natural frequency w_n the constants of $R(x)$ and $S(x)$ should be determined; but β_n causes the rows of D_n to be linearly dependent and its determinant to be zero. For this reason by arbitrarily choosing one of the constants and omitting one of the suitable equations, a system of equations with 7 unknowns and 7 linearly independent equations can be obtained. Then, the constants and then the mode shape scaled by one of the constants can be determined. Finally, the arbitrarily chosen constant can be calculated from the constants of the temporal equation (Equation 2.8) and the initial conditions.

2.3 Orthogonality of the Natural Modes for Multi-Stepped Beams

For a uniform single span beam it is easy to prove the orthogonality condition for any n^{th} and m^{th} modes of the beam as [22]

$$\int_0^l Y_n(x).Y_m(x).dx = 0 \tag{2.31}$$

where l is the length of the beam.

However, in case of a multi-stepped beam, due to step changes in the cross section orthogonality must be modified. When Equation (2.5) is substituted into Equation (2.1) and the free vibration is considered with constant density and modulus of elasticity, it yields

$$\frac{1}{\rho.A(x).Y_n(x)}.\frac{d^2}{dx^2}\left[E.I(x).\frac{d^2Y_n(x)}{dx^2}\right] = -\frac{1}{T_n(t)}.\frac{d^2T_n(t)}{dt^2} = {w_n}^2 \tag{2.32}$$

rearranging this equation one can get

$$\frac{d^2}{dx^2}\left[E.I(x).\frac{d^2Y_n(x)}{dx^2}\right] - {w_n}^2.\rho.A(x).Y_n(x) = 0 \tag{2.33}$$

and for the mth mode

$$\frac{d^2}{dx^2}\left[E.I(x).\frac{d^2Y_m(x)}{dx^2}\right] - {w_m}^2.\rho.A(x).Y_m(x) = 0 \tag{2.34}$$

Multiplying the Equation (2.33) by $Y_m(x)$ and the Equation (2.34) by $Y_n(x)$, subtracting the resulting equations and then integrating side by side the following is obtained

$$\begin{gathered}\frac{\rho.({w_m}^2 - {w_n}^2)}{E}.\int_0^l \left[A(x).Y_n(x).Y_m(x)\right]dx = \Re \\ \Re = \int_0^l \left[Y_m(x)\frac{d^2}{dx^2}\left[I(x).\frac{d^2Y_n(x)}{dx^2}\right] - Y_n(x)\frac{d^2}{dx^2}\left[I(x).\frac{d^2Y_m(x)}{dx^2}\right]\right].dx\end{gathered} \tag{2.35}$$

Since $w_m \neq w_n$, if $\Re$ is zero orthogonality condition is proved. With ${Y_n}^I$ standing for the first derivative of $Y_n(x)$ with respect to x and so on for the others

$$\begin{aligned}\Re = \int_0^l \Big[&Y_m.(I^{II}.{Y_n}^{II} + 2I^I.{Y_n}^{III} + I.{Y_n}^{IIII}) \\ &- Y_n.(I^{II}.{Y_m}^{II} + 2I^I.{Y_m}^{III} + I.{Y_m}^{IIII})\Big]dx\end{aligned} \tag{2.36}$$

rearranging Equation (2.36) in terms of multiples of I and its derivatives one obtains:

$$\Re = \int_0^l \Big[I^{II}.(Y_n{}^{II}.Y_m - Y_m{}^{II}.Y_n) + 2I^{I}.(Y_n{}^{III}.Y_m - Y_m{}^{III}.Y_n) + I.(Y_n{}^{IIII}.Y_m - Y_m{}^{IIII}.Y_n) \Big] dx \tag{2.37}$$

taking the integration

$$\Re = \Big(I(Y_n{}^{III}.Y_m - Y_m{}^{III}.Y_n + Y_m{}^{II}.Y_n{}^{I} - Y_n{}^{II}.Y_m{}^{I}) + I^{I}(Y_n{}^{II}.Y_m - Y_m{}^{II}.Y_n) \Big|_o^l \tag{2.38}$$

Since for any boundary condition the bending moment and slope, and the shear force and deflection cannot be zero at the same time; and also since I^I is zero at the end conditions, for all of the coefficients of Equation (2.38) there is a vanishing element that makes it zero. So the orthogonality condition for multi-stepped beams is proved.

$$\int_0^l \big[A(x).Y_n(x).Y_m(x) \big] dx = 0 \tag{2.39}$$

Note that due to the step change in cross section there is a term of $A(x)$ in the equation of orthogonality.

2.4 Forced Vibration of Multi-Stepped Beams

For analyzing the forced vibration of a beam the modal analysis method is applied. The total response of the beam is the sum of its responses in all modes [21].

$$y(x,t) = \sum_{n=1}^{\infty} Y_n(x).T_n(t) \tag{2.40}$$

2.4.1 Undamped Forced Vibration

In this section, structural damping of the beam is neglected for forced response analysis.

Application of Equation (2.40) into the Equation (2.1) yields

$$\rho.\sum_{n=1}^{\infty} A(x).Y_n(x).\frac{d^2T_n(t)}{dt^2} + T_n(t).\frac{d^2}{dx^2}\left(E.I(x).\sum_{n=1}^{\infty} \frac{d^2Y_n(x)}{dx^2} \right) = f(x,t) \tag{2.41}$$

substituting equation (2.33)

$$\sum_{n=1}^{\infty} A(x).Y_n(x).\frac{d^2T_n(t)}{dt^2} + T_n(t)\sum_{n=1}^{\infty} {w_n}^2.A(x).Y_n(x) = \frac{f(x,t)}{\rho} \tag{2.42}$$

By multiplying Equation (2.42) with $Y_m(x)$, integrating from 0 to l and using the orthogonality condition, Equation (2.39), the following is obtained

$${w_n}^2.T_n(t) + \frac{d^2T_n(t)}{dt^2} = \frac{Q_n(t)}{\rho.b_n} \tag{2.43}$$

where the constant b_n is defined as

$$b_n = \int_0^l A(x).{Y_n}^2(x).dx \tag{2.44}$$

and

$$Q_n(t) = \int_o^l f(x,t).Y_n(x).dx \tag{2.45}$$

Equation (2.43) is the same as the case of an undamped system. By means of *convolution integral* for any excitation of $f(x,t)$, response of the system can be determined. On the other hand, since it is dealt with frequency response function of the system it is assumed that the excitation is a real harmonic excitation applied on any point of the beam and is like a function of time $f(t) = f_0.\cos(wt)$.

With the harmonic force of $f(t) = f_0.\cos(wt)$ applied on the beam at $x = x_1$ one can obtain

$$T_n(t) = \frac{f_0.Y_n(x_1)}{\rho.b_n.({w_n}^2 - w^2)}.\cos(wt) \tag{2.46}$$

Multiplying Equation (2.46) with the corresponding mode shape and then adding up for all modes $y(x,t)$, (Equation 2.40) can be obtained as

$$y(x,t) = \sum_{n=1}^{\infty} Y_n(x).\frac{f_0.Y_n(x_1)}{\rho.b_n.({w_n}^2 - w^2)}.\cos(wt) \tag{2.47}$$

As a result it yields that for a beam excited at $x = x_1$ with a harmonic force of $f(t) = f_0.\cos(wt)$, the deflection response at $x = x_2$ is

$$y(x_2,t) = \sum_{n=1}^{\infty} Y_n(x_2).\frac{f_0.Y_n(x_1)}{\rho.b_n.({w_n}^2 - w^2)}.\cos(wt) \tag{2.48}$$

which brings the frequency response function as $H_{x1x2} = y(x,t)/f(x,t)$

$$H_{x1x2} = \sum_{n=1}^{\infty} Y_n(x_2).\frac{Y_n(x_1)}{\rho.b_n.(w_n{}^2 - w^2)} \tag{2.49}$$

2.4.2 Damped Forced Vibration

Damping caused by the friction between the internal planes that slip as the material deforms is called structural (or hysteretic) damping. From the literature it is known that the energy dissipated per cycle of motion for a system with hysterical damping is independent of frequency, and the equivalent viscous damping coefficient and damping ratio are [23]

$$c_{eq} = \frac{h.k}{w} \text{ and } \zeta = \frac{h.w_n}{2.w} \tag{2.50}$$

where h is the hysteretic damping constant. Note that this equation is valid only for harmonic excitation.

A simple procedure for including damping to a continuous system is to add it to the temporal equation after separation of variables. In modal parameters adding the term

$$2\zeta_n.w_n.\frac{dT_n(t)}{dt} \tag{2.51}$$

into Equation (2.43) it yields

$$w_n{}^2.T_n(t) + 2\zeta_n.w_n.\frac{dT_n(t)}{dt} + \frac{d^2T_n(t)}{dt^2} = \frac{Q_n(t)}{\rho.b} \tag{2.52}$$

which is in the form of a forced vibration of a damped system. The forced response of a damped system is of the form of a harmonic function of the same frequency as excitation force but with a different amplitude and phase. The phase shift is expected because of the effect of the damping force. The solution of Equation (2.52), for the same force function and the same locations of force and response as described in the previous section, is

$$T_n(t) = \frac{f_0.Y_n(x_1)}{\rho.b.\sqrt{(w_n{}^2 - w^2)^2 + (2\zeta_n.w_n.w)^2}}.\cos(wt - \tan^{-1}\frac{2\zeta_n.w_n.w}{w_n{}^2 - w^2}) \tag{2.53}$$

Substituting Equation (2.50) into Equation (2.53) results

$$T_n(t) = \frac{f_0.Y_n(x_1)}{\rho.b.\sqrt{(w_n{}^2 - w^2)^2 + (h.w_n{}^2)^2}}.\cos(wt - \tan^{-1}\frac{h.w_n{}^2}{w_n{}^2 - w^2}) \tag{2.54}$$

Multiplying Equation (2.54) with the corresponding mode shape and then adding up for all modes, the response at $x = x_2$ can be obtained as

$$y(x_2,t) = \sum_{n=1}^{\infty} Y_n(x_2).\frac{f_0.Y_n(x_1)}{\rho.b.\sqrt{({w_n}^2 - w^2)^2 + (h.{w_n}^2)^2}}.\cos(wt - \tan^{-1}\frac{h.{w_n}^2}{{w_n}^2 - w^2}) \quad (2.55)$$

And from Equation (2.55) the amplitude and the phase of the frequency response function for mode n is

$$A_n = Y_n(x_2).\frac{Y_n(x_1)}{\rho.b.\sqrt{({w_n}^2 - w^2)^2 + (h.{w_n}^2)^2}} \quad (2.56)$$

and

$$\phi_n = \frac{h.{w_n}^2}{{w_n}^2 - w^2} \quad (2.57)$$

respectively. So the amplitude and the phase of the total frequency response function become

$$A = \sqrt{\left(\sum_{n=1}^{\infty} A_n.\cos(\phi_n)\right)^2 + \left(\sum_{n=1}^{\infty} A_n.\sin(\phi_n)\right)^2} \quad (2.58)$$

and

$$\phi = \tan^{-1}\left(\frac{\sum_{n=1}^{\infty} A_n.\sin(\phi_n)}{\sum_{n=1}^{\infty} A_n.\cos(\phi_n)}\right) \quad (2.59)$$

Damping force at the supports, in fact, is usually more important for consideration. It is possible to treat the damping forces at the supports as external forces and to include in the calculation of $Q_n(t)$ with a minus sign in front. Assuming that the damping ratios are same for all supports the generalized damping force can be written as

$$c.\frac{\partial y(x.t)}{\partial t} = c.Y(x).\frac{dT(t)}{dt} \quad (2.60)$$

Substituting this damping force equation into Equation (2.45) for the supports located at $x = x_3$ and $x = x_4$ $Q_n(t)$ results

$$Q_n(t) = f_0.\cos(w.t).Y_n(x_1) - c.\frac{dT_n(t)}{dt}({Y_n}^2(x_3) + {Y_n}^2(x_4)) \quad (2.61)$$

And also since

$$\frac{c}{\rho.\int_0^l A(x).dx} = 2\zeta_s.w_n \tag{2.62}$$

where ζ_s stands for the damping ratio of the supports which is constant, the Equation (2.52) takes the form of

$$w_n{}^2.T_n(t) + 2w_n.\left[\zeta_n + \frac{\zeta_s.\left(Y_n{}^2(x_3) + Y_n{}^2(x_4)\right)\int_0^l A(x).dx}{b}\right].\frac{dT_n(t)}{dt} + \frac{d^2T_n(t)}{dt^2} = \frac{f_0.\cos(w.t).Y_n(x_1)}{\rho.b} \tag{2.63}$$

Using an equivalent damping ratio as

$$\zeta_{eq} = \frac{h.w_n}{2.w} + \frac{\zeta_s.\left(Y_n{}^2(x_3) + Y_n{}^2(x_4)\right)\int_0^l A(x).dx}{b} \tag{2.64}$$

the solution of the temporal equation becomes

$$T_n(t) = \frac{f_0.Y_n(x_1)}{\rho.b.\sqrt{(w_n{}^2 - w^2)^2 + (2\zeta_{eq}.w_n.w)^2}}.\cos(wt - \tan^{-1}\frac{2\zeta_{eq}.w_n.w}{w_n{}^2 - w^2}) \tag{2.65}$$

Multiplying Equation (2.65) with the corresponding mode shape and then adding up for all modes, the response at $x = x_2$ can be obtained as

$$y(x_2,t) = \sum_{n=1}^{\infty}\left(Y_n(x_2).\frac{f_0.Y_n(x_1)}{\rho.b.\sqrt{(w_n{}^2 - w^2)^2 + (2\zeta_{eq}.w_n.w)^2}}.\cos(wt - \tan^{-1}\frac{2\zeta_{eq}.w_n.w}{w_n{}^2 - w^2})\right) \tag{2.66}$$

And from Equation (2.66) the amplitude and the phase of the frequency response function for mode n is

$$A_n = Y_n(x_2).\frac{Y_n(x_1)}{\rho.b.\sqrt{(w_n{}^2 - w^2)^2 + (2\zeta_{eq}.w_n.w)^2}} \tag{2.67}$$

and

$$\phi_n = \frac{2\zeta_{eq}.w_n.w}{{w_n}^2 - w^2} \tag{2.68}$$

respectively. So the amplitude and the phase of the total frequency response function become

$$A = \sqrt{\left(\sum_{n=1}^{\infty} A_n.\cos(\phi_n)\right)^2 + \left(\sum_{n=1}^{\infty} A_n.\sin(\phi_n)\right)^2} \tag{2.69}$$

and

$$\phi = \tan^{-1}\left(\frac{\sum_{n=1}^{\infty} A_n.\sin(\phi_n)}{\sum_{n=1}^{\infty} A_n.\cos(\phi_n)}\right) \tag{2.70}$$

For the described analysis of the beam supported at the mid positions, the effects of structural damping of the beam and damping of the supports on the mode shapes of the beam are neglected. The reason is that since the modes shapes are found from the spatial equations, it is not possible to add the effect of any damping which is proportional with the first derivative of the deflection with respect to time.

3 CONTACT STIFFNESS

Stiffness is the capacity of a mechanical system to sustain loads without permanent changes of its geometry. It is one of the most important design criteria for mechanical components and systems. Although strength is considered as the most important design criterion, there are many cases in which stresses in components and their connections are significantly below the allowable levels, and dimensions as well as performance characteristics of mechanical systems and their components are determined by stiffness requirements.

It is worthwhile to introduce some types of stiffness:

- Structural stiffness due to deformations of a part or a component considered as beam, plate, shell, etc.
- Contact stiffness due to deformations in a connection between two components.

Since stiffness is the ratio of the force to the displacement caused by this force, the load-deflection characteristic allows one to determine stiffness as a function of force. It is much easier to analyze both static and dynamic structural problems if the displacements are proportional to the forces that caused them. However, most load-deflection characteristics of actual mechanical systems are nonlinear. In many cases the degree of nonlinearity is not very significant and the system is considered as linear for the sake of simplicity.

One specific example of nonlinear stiffness is the one due to contact deformations. In contact deformations, joints loaded perpendicularly to the contact surface are characterized by a hardening nonlinearity due to increase of effective contact area with the increasing load.

When components with different curvature radii are compressed together, the contact area is small because of their geometry. Finite element model of deformation zone is as in the following figure.

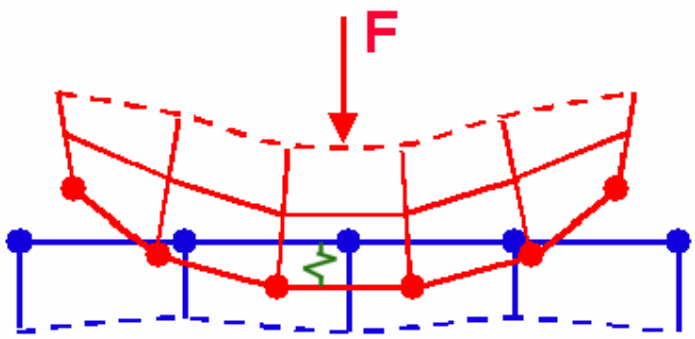

Figure 3.1: FEM of contact deformation.

On the other hand for the case of the cylindrical connections contact area is not so small. For this reason contact deformations in cylindrical connections cannot be analyzed by Hertz formulas since those were derived for cases where the contact area is small in relation to curvature radii of the contacting bodies.

Contact deflections in cylindrical joints depend on the clearance magnitude. Since an increased clearance means a greater difference in curvature radii and, as a result, a reduction in the contact arc, it also leads to a steep increase in contact deformations.

3.1 Cylindrical Connections with Clearance Fit

In cylindrical connections with clearance fits, respective radii r_1 and r_2 of the hole and pin surfaces are very close to each other. The clearance per diameter $\Delta = 2(r_1 - r_2)$ is several orders of magnitude smaller than r_1 and r_2. Although Hertz formulas are not applicable in such cases, they can be used as an approximation when loads are small and clearances are relatively large. For a more general case of higher loads and smaller clearances, deformations of the housing in which the hole is made are important.

In the analysis it is assumed that both the pin and the hole are perfectly smooth, but real parts have micro asperities and waviness whose deformations may add significantly to the overall deformations.

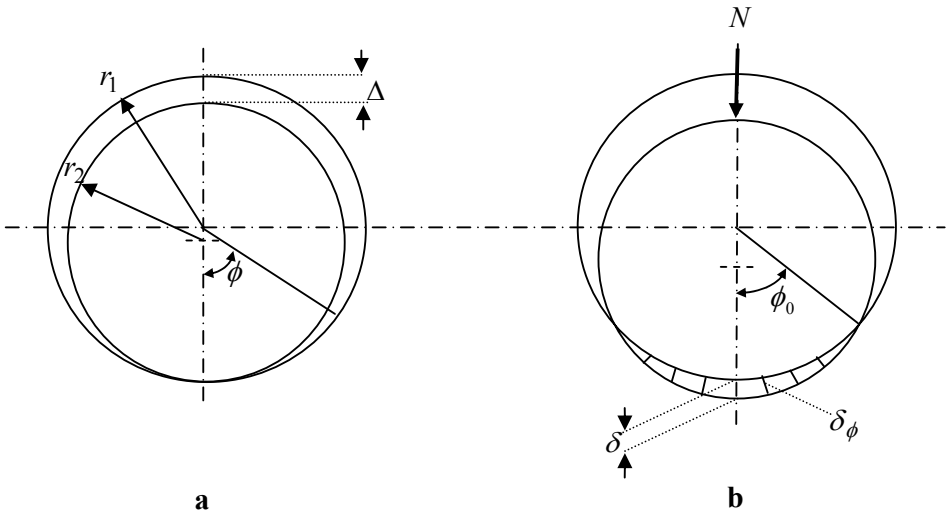

Figure 3.2: Model for analysis of contact deformation of cylindrical connections with clearance: (a) initial contact; (b) contact under load.

In Figure 3.2, N, in N/m, is load per unit length of connection ($L_{contact}$). Displacement δ caused by external force is along the direction of the force N. ϕ_0 is the contact angle. Radial displacement at angle ϕ is δ_ϕ.

Under external loading of connection, total pressure on one side is increasing, while on the opposite side it is decreasing. Maximum displacement caused by external force is along the direction of the force.

Two correlations (linear and nonlinear contact deformations) between contact pressure p and deformation δ are considered [24].

$$\delta = k.p \tag{3.1}$$

and

$$\delta = c.p^m \tag{3.2}$$

where k and c are constant, and exponent of pressure p is an empirical constant for the contact between two surfaces of different or same material, for example $m = 0.5$ for contacting steel and cast iron surfaces [24].

Assuming the distributions of radial clearance and displacement are cosinusoidal following expressions can be obtained. The radial clearance at angle ϕ is

$$\Delta_\phi = 0.5\Delta.(1 - \cos(\phi)) \tag{3.3}$$

Elastic radial displacement at angle ϕ in the direction acting of load N

$$\delta_\phi = \delta.\cos(\phi) - \Delta_\phi \tag{3.4}$$

where δ is the displacement in the direction of the load N.

3.1.1 Linear Contact Compliance

In the case of linear contact compliance, deformation as a function of ϕ and p is

$$\delta_\phi = k.p_\phi \tag{3.5}$$

where k is the contact compliance coefficient. The vertical component of contact pressure at angle ϕ is

$$p_{\phi\_ver} = p_\phi.\cos(\phi) \tag{3.6}$$

substituting Equations (3.3), (3.4) and (3.5) in Equation (3.6);

$$\begin{aligned} p_{\phi\_ver} &= \frac{1}{k}.\left(\delta.\cos(\phi) - 0.5\Delta.(1-\cos(\phi))\right).\cos(\phi) \\ \Rightarrow p_{\phi\_ver} &= \frac{1}{2k}.\left((2\delta+\Delta).\cos^2(\phi) - \Delta.\cos(\phi)\right) \end{aligned} \tag{3.7}$$

The total vertical load denoted by N can be obtained by integrating p_{ϕ_ver} along the contact arc $2\phi_0$

$$\int p_{\phi\_ver}.ds = \int p_{\phi\_ver}.r.d\phi \tag{3.8}$$

where s is the arc length and r is the nominal radius. Rearranging Equation (3.8) one obtains:

$$N = \frac{r}{2k}.\int_{-\phi_0}^{\phi_0} \left[(2\delta+\Delta).\cos^2(\phi) - \Delta.\cos(\phi)\right] d\phi \tag{3.9}$$

integrating

$$N = \frac{r.(2\delta+\Delta)}{k}.\left[\frac{\cos(\phi_0).\sin(\phi_0)+\phi_0}{2} - \frac{\Delta.\sin(\phi_0)}{(2\delta+\Delta)}\right] \tag{3.10}$$

Half angle of contact arc ϕ_0 is determined from the condition that

$$\delta_{\phi_0} = 0 \tag{3.11}$$

From Equations (3.3) and (3.4) this yields

$$\delta.\cos(\phi_0) - 0.5\Delta.(1-\cos(\phi_0)) = 0$$
$$\Rightarrow \cos(\phi_0) = \frac{\Delta}{2\delta + \Delta} \tag{3.12}$$

Substituting Equation (3.12) and the nominal diameter $d = 2r$ in Equation (3.10) one can get

$$N = \frac{r.(2\delta + \Delta)}{k}.\left[\frac{\cos(\phi_0).\sin(\phi_0) + \phi_0}{2} - \cos(\phi_0).\sin(\phi_0)\right]$$
$$N = \frac{d}{4k}.(2\delta + \Delta).(\phi_0 - \cos(\phi_0).\sin(\phi_0)) \tag{3.13}$$

Thus, for the determination of the two unknowns of δ and ϕ_0 Equations (3.12) and (3.13) can be used.

Maximum pressure in the direction of force which is obviously δ / k is

$$p_{\max} = p_{av}\left[2(1-\cos(\phi_0))\right]/(\phi_0 - \sin(\phi_0)\cos(\phi_0)) \tag{3.14}$$

where $p_{av} = q / d$ (note that it is not in fact average pressure in the contact zone, it is only a given definition to calculate $p_{\max}$).

If there is no clearance, then $\Delta = 0$ and

$$\phi_0 = \frac{\pi}{2} \quad , \quad \delta = \frac{4k.N}{\pi.d} \quad \text{and} \quad p_{\max} = \frac{4p_{av}}{\pi} \tag{3.15}$$

3.1.2 Nonlinear Contact Compliance

In the case of nonlinear contact compliance, deformation as a function of ϕ and p is

$$\delta_\phi = c.p_\phi^{0.5} \tag{3.16}$$

where c is the contact compliance coefficient. Then analogously,

$$p_{\phi\_ver} = \frac{(\delta.\cos(\phi) - 0.5\Delta.(1-\cos(\phi)))^2.\cos(\phi)}{c^2} \tag{3.17}$$

and then integrating p_{ϕ_ver} along the contact arc $2\phi_0$

$$N = \frac{r}{c^2}.\left[\left(\delta^2 + \delta.\Delta + \frac{\Delta^2}{4}\right).\left(\frac{\cos^2(\phi).\sin(\phi) + 2\sin(\phi)}{3}\right)\right.$$
$$\left. -\left(\frac{4\delta.\Delta + \Delta^2}{4}\right).\left(\cos(\phi).\sin(\phi) + \phi\right) + \frac{\Delta^2}{4}\sin(\phi)\right]_{-\phi_0}^{\phi_0} \tag{3.18}$$

Substituting ϕ_0 and using Equation (3.12), one can rewrite Equation (3.18) as:

$$N = \frac{r}{2c^2}.(2\delta + \Delta)^2.\left(\sin(\phi_0) - \frac{\sin^3(\phi_0)}{3} - \phi_0.\cos(\phi_0)\right) \tag{3.19}$$

Two unknowns, δ and ϕ_0 can be determined by solving Equations (3.12) and (3.19).

The empirical constants *k* for linear and *c* for nonlinear contact compliances can be obtained from literature for various clearances and materials. Then using any of the relations (3.13) and (3.19), one can easily get the force-deflection relation.

3.2 Stiffness of Ball Bearings

Stiffness of a bearing is the inverse of the rate of change of bearing deflection with applied load. In order to find the stiffness of a particular rolling bearing under a given type of loading, one first determine the load distribution among the rolling elements and then relate the maximum rolling element load to the applied load.

Stiffness of rolling element bearings is dependent on the internal clearance, size and number of rolling elements and if applicable on the preload as illustrated in Figure 3.3. In the following analysis it is assumed that there is no radial clearance in the bearing and the bending deformation of the bearing races are negligible since they are supported by the housing or the shaft.

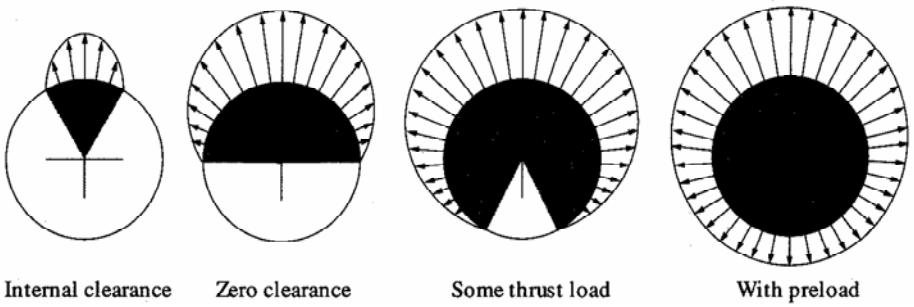

Figure 3.3: Effect of bearing preload on the bearing load distribution [25].

From the Hertz contact theory equations, for a spherical contact to any plane or curved surface the deflection has the following proportional relationship to the applied force [26]

$$\delta^b = C.F^{2/3} \tag{3.20}$$

where δ^b is the deformation, F applied force and C is a constant depending on the geometries of the contacting surfaces.

C can be determined for the contact of two surfaces with curvatures by means of the formula [25]

$$C = \frac{1}{2}.\left(\frac{9}{4R_e.E_e{}^2}\right)^{1/3} \tag{3.21}$$

where R_e and E_e are equivalent radius and modulus of elasticity of the system, respectively.

The equivalent radius of the system is found from

$$R_e = \frac{1}{\frac{1}{R_{1_{major}}} + \frac{1}{R_{1_{\min or}}} + \frac{1}{R_{2_{major}}} + \frac{1}{R_{2_{\min or}}}} \tag{3.22}$$

where the major and minor radii are the surface radii around the two axis which are parallel to the contact plane. Note that convex surfaces' radii are positive, concave surfaces' radii are negative, and flat plane radii are infinite.

The equivalent modulus of elasticity of the system based on the elastic modulii and Poisson ratios of the two materials in contact can be obtained from

$$E_e = \frac{1}{\frac{1-\nu_1{}^2}{E_1} + \frac{1-\nu_2{}^2}{E_2}} \tag{3.23}$$

Radial load F_r applied to a ball bearing is distributed nonuniformly between the rolling elements as shown in Figure 3.4. If the bearing is not preloaded, the load is applied only to the balls located within the arc, not exceeding 180 degree as shown in the figure.

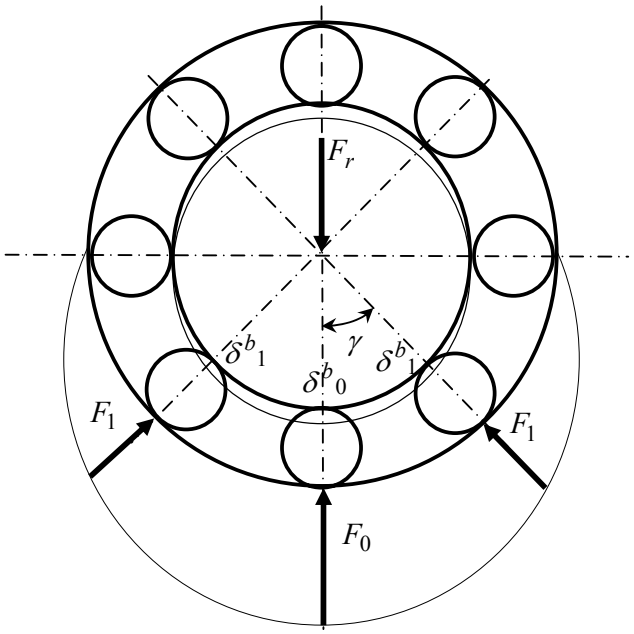

Figure 3.4: Model of load distribution between rolling bodies.

The most loaded ball is one located on the vector of the radial load F_r. The force acting on the most highly loaded central ball is F_0. The forces on the balls located at a pitch angle of γ to the load vector is F_1, for the ones located at 2γ is F_2 and so on. Here γ is the angle between the adjacent balls, and with z being the total number of balls it is equal to

$$\gamma = \frac{360}{z} \tag{3.24}$$

It can be assumed that the radial displacement between the races at each ball, caused by contact deformations of the balls and races, are equal to projections of the total displacement δ_0^b of the inner race along the direction of applied load as

$$\delta_1^b = \delta_0^b.\cos(\gamma), \quad \delta_2^b = \delta_0^b.\cos(2\gamma), \ldots \quad \delta_i^b = \delta_0^b.\cos(i.\gamma) \tag{3.25}$$

where i is the number of the ball.

3.2.1 Deep Groove Ball Bearings

Since for deep groove ball bearings there is no preloading, loading is as shown in Figure 3.4 and one half of the balls are located in the loaded zone (No internal clearance assumed).

Substituting Equation (3.20) into Equation (3.25) one can get

$$F_1 = F_0.\cos^{3/2}(\gamma), \quad F_2 = F_0.\cos^{3/2}(2\gamma), \ldots \quad F_i = F_0.\cos^{3/2}(i.\gamma) \tag{3.26}$$

The equilibrium condition requires that the radial load F_r is balanced by reactions of the loaded balls. And assuming symmetrically located balls relative to the plane of radial load, F_r can be obtained as

$$F_r = F_0.\left(1 + 2\sum_{i=1}^{i=z/4}\cos^{5/2}(i.\gamma)\right) \tag{3.27}$$

By means of this equation one can obtain F_0, and then substituting it into Equation (3.20) total displacement δ_0^b of the inner race can be found.

3.2.2 Angular Contact Ball Bearings

Angular contact ball bearings are suitable for high speeds, and can accommodate radial and thrust (in only one direction) loads. In spindle systems spindle bearings, which are specially designed angular contact ball bearings differing in contact angle, tolerances and cage design, are used.

Forces acting on an angular contact ball bearing are as shown in Figure (3.5):

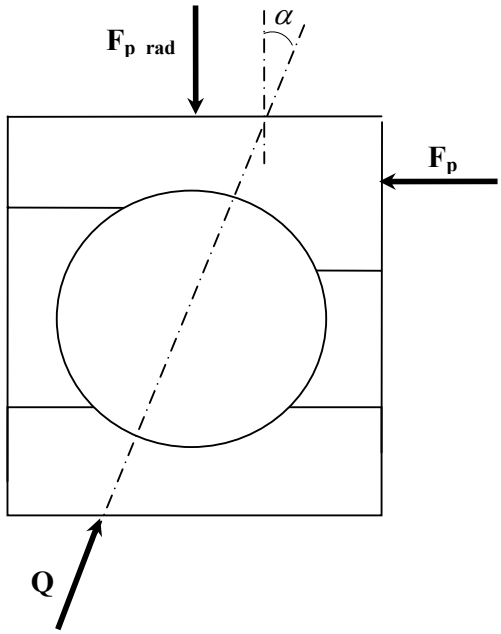

Figure 3.5: Forces acting on an angular contact ball bearing.

where α is the contact angle, Q is the load along the line of contact, F_p is the preload, and when there is no resisting friction force against the preload

$$F_{p\_rad} = \frac{F_p}{\tan(\alpha)} \tag{3.28}$$

If the bearing is preloaded, each rolling body is loaded by the radial force F_{p-rad}. As a result all rolling bodies are participating in the loading process. And for the external loading case in Figure 3.4 the bodies in the lower half are experiencing increase of their radial loading and the ones in the upper half are experiencing reduction of their radial loading as shown in the last part of Figure 3.3.

Initial deformation due to preload is given by

$$\delta^b_{preload} = C.\left(\frac{F_{p\_rad}}{z}\right)^{2/3} \tag{3.29}$$

Using the same assumption made for equation (3.25) for the deformation due to external loading, one can write the forces on the rolling bodies as

$$F_i = \left(\frac{\delta^b_{preload} + \delta^b_{00}.\cos(i.\gamma)}{C}\right)^{3/2} \tag{3.30}$$

where δ^b_{00} is the total displacement of the inner race.

Again the equilibrium of the radial load F_r and the reactions forces of the balls should be satisfied.

$$F_r = \sum_{i=0}^{z-1} F_i . \cos(i.\lambda) \tag{3.31}$$

from which the total displacement δ_{00}^{b} of the inner race can be found easily.

3.3 Preload Force Equilibrium of Rotor-Bearing Systems

In many applications, rolling bearings must be treated as integral parts of the system to be able to accurately determine shaft deflections, dynamic shaft loading and also the performance of the bearings. Load distribution of the bearings is affected by the radial and angular deflections of the shaft and loads applied on any system component.

Since self-aligning capability of angular contact ball bearings or spindle bearings is very limited, the effect of radial and angular deflections of the shaft can be assumed to be changing the loads of the bearings without any change in the contact angle.

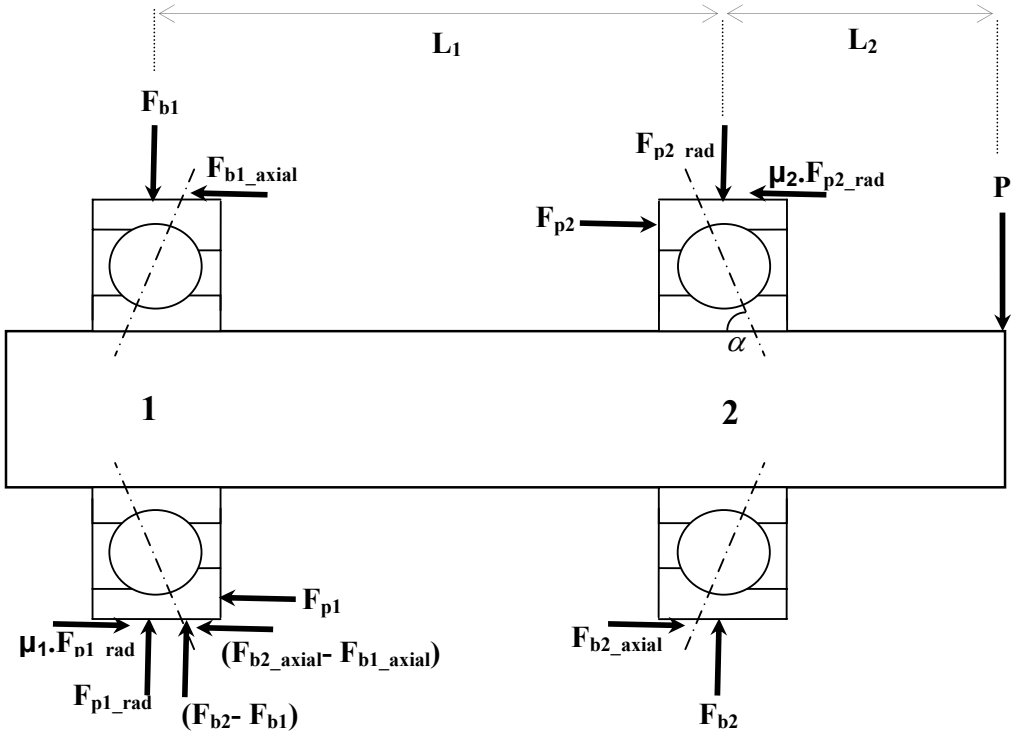

Figure 3.6: Free body diagram of the shaft supported with angular contact ball bearings.

The system with a back-to-back configuration of the bearings is shown in the Figure 3.6 in which friction forces are also taken into consideration. In the figure, for the bearing in position-1, the upper part, and for the bearing in position-2, the lower part, show the bearing loads due to the external load P. The upper part of bearing-2 shows the forces distributed uniformly along the circumference of the bearing due to the initial preload F_{p2}.

On the other hand, the case for the lower part of the bearing-1 is a little different. For the case shown in the figure, F_{b2} will be much higher than F_{b1}. Since these forces result from the axial loads due to the contact angles of the bearings, the axial load F_{b2_axial} exceeds the axial load F_{b1_axial}. This unbalance in axial forces results a uniformly distributed load on bearing-1. The lower part of the bearing-1 shows the effects of this unbalance and the initial preload F_{p1}.

With the assumption of a rigid shaft following relations between the applied forces and the bearing loads can be obtained:

- Equations for the moment about bearing-2 and the vertical forces yield respectively

$$\begin{aligned} P.L_2 &= F_{b1}.L_1 \\ P + F_{b1} &= F_{b2} \end{aligned} \tag{3.32}$$

- From the contact angles of the bearings which are assumed to be the same one obtains

$$\begin{aligned} \tan(\alpha) &= \frac{F_{b1\_axial}}{F_{b1}} = \frac{F_{b2\_axial}}{F_{b2}} \\ \tan(\alpha) &= \frac{F_{p1} - \mu_1.F_{p1\_rad}}{F_{p1\_rad}} = \frac{F_{p2} - \mu_2.F_{p2\_rad}}{F_{p2\_rad}} \end{aligned} \tag{3.33}$$

- Also for the unloaded condition of $P = 0$, from the equality of the axial forces one can write

$$F_{p1\_rad} = F_{p2\_rad} \tag{3.34}$$

By means of Equations (3.32-33 and 34) one can get seven linearly independent equations for the unknowns F_{p1_rad}, F_{p2_rad}, F_{b1}, F_{b2}, F_{b1_axial}, F_{b2_axial}, μ_1 and μ_2. Hence, the system is a statically indeterminate system, as we have only seven

equations for eight unknowns, some experimental data is needed for the determination of the unknowns.

A static deflection analysis of the total system including all of the parameters of the bearings, housing and spindle can be done with the analysis described in this chapter. But when the friction forces are included in the analysis one unknown remains undetermined.

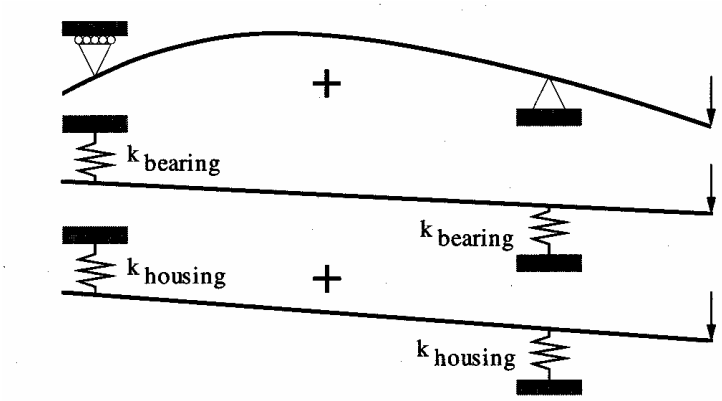

Figure 3.7: Sources of deflection in a shaft, bearings and housing system.

From the experimental data of the deformation of the whole shaft, bearings and housings system, and equating it to the sum of the deformations of the shaft, bearings and housings as described in Figure 3.7, one can easily obtain the remaining unknown.

For a system as shown in Figure 3.7 the shaft deformation can be analytically calculated or obtained by means of finite element methods. For the calculation of the deformations of the housings, one should take the vertical loads as F_{b1} and F_{b2} as in the case of Figure 3.6. Finally to calculate the bearing deformations one should take the radial preload force F_{p-rad} as $(F_{p1-rad} + F_{b2} - F_{b1})$ for the first bearing and F_{p2-rad} for the second bearing with the applied radial loads of F_{b1} and F_{b2} respectively.

4 IMPLEMENTATION OF ANALYTICAL MODELS AND COMPARISON WITH FINITE ELEMENT ANALYSIS

This chapter provides the practical implementation of analytical models described in the chapters two and three, and comparison of these with finite element modelling. The proposed mathematical model assumes that the rotor-bearing system consists of a series of rigidly connected, multi-stepped beams supported on springs and dampers. The proposed model is capable of predicting the frequencies, mode shapes and the deflection/force frequency response of any rotor with n-steps and m-supports. Moreover, the contact stiffness model allows determining the stiffness between the rotor and the supports. The model is used for determination of the transverse dynamics parameters of a rotor-bearing system with rigid supports and well defined dimensions. To date, within best of author's knowledge, the methodology developed here represents a novel technique.

This chapter consists of a short explanation of the methodology used in the analytical model starting from a simple free-free beam and extending to a multi-stepped rotor supported on the springs and dampers; and comparisons of the model with FEM.

4.1 Implementation of Analytical Models

Rotor deflection and bearing stiffness are calculated by the models implementation in MATLAB as described in the previous chapters. Analysis of the whole rotor-bearing system with some essential assumptions is accomplished by means of an additional code which utilizes the previous ones.

Frequencies and mode shapes of the rotor are determined with the application of free vibration analysis. It is assumed that every support or bearing divides a section into two sub-sections, and as a result adds a new section to the system. Following the setting

of material properties and dimensions of the rotor, a simple beam model is applied to each of those sections with different β_n values (n stands for the nth mode) as described in Equation (2.10). The β_n values can be written in terms of eigenfrequencies and in the form of a system of equations for each beam subject to boundary conditions as described in the example in Section 2.2.2. Then, one can treat the problem as a root finding problem for a set of nonlinear equations. The determined roots are used to calculate the corresponding frequencies and mode shapes. However, note that, determination of the roots, usually after the third root in case of complex geometries, is not always guaranteed as the hyperbolic functions, sinh and cosh, may diverge to infinity.

For the forced response of the rotor, the forced vibration results of a multi-stepped beam in section 2.4 can be utilized by means of simple codes in MATLAB. In the case of the prediction of the connection stiffness between the rotor and the supports, equations derived in Chapter 3 can be applied by means of relatively simple programming in MATLAB. Combining these equations with the experimental data, estimation of the friction coefficient between the outer ring of the bearing and the housing is explained in the following sections.

4.2 Finite Element Analysis

The principal advantage of the finite element method is its generality and accuracy. It can be used to determine the natural frequencies and mode shapes of any linear, elastic structure which may have no analytical solution. On the other hand, FEM calculations can be extremely prohibitive for complex objects and computational resources may run out quickly.

For the Finite Element Analysis (FEA) of the rotors used in the thesis, *FEMLAB 3.0a* [27] is used.. Creating the 3-D model of the rotor, its frequencies, mode shapes and FRFs are obtained by means of the tools *Eigen Frequency Analysis* and F*requency Response Analysis* of *FEMLAB 3D-Structural Mechanics Module.* For the numerical solution of the linear system of equations, *Direct (SPOOLES)* which solves the linear systems by Gaussian elimination, is invoked as preferred solver in the FEMLAB.

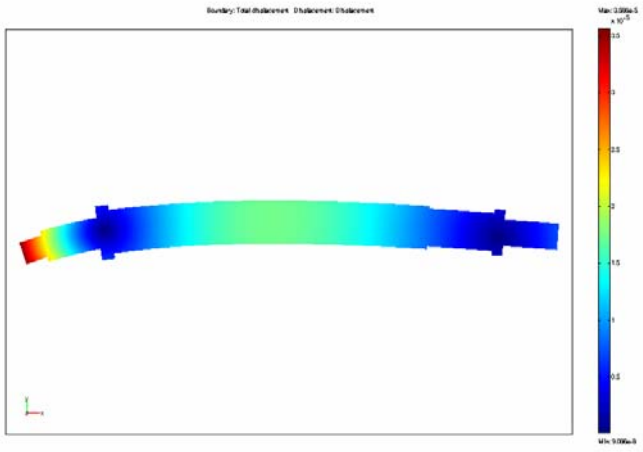

Figure 4.1: FEA of a multi-stepped beam under a static load at the left end.

An example of FEA of a multi-stepped beam of the same sizes with the experimental shaft and supported with two bearings can be seen in Figure 4.1. A static force of 900 N is applied at the left end of the beam, which causes more deflection at the left, as it is seen in colour red. Static deflection of the left end is obtained as *35,66e-6* .

FEMLAB uses a tetrahedral mesh in 3D structures. Not only the shape of the mesh but also the number of nodes in the mesh has a great effect on obtaining the correct results. Finer mesh structures give closer results to real life applications. In the FEM simulations as fine mesh as possible is used within the limits of a 2GB RAM of an HP6000 series workstation. The accuracy of the FEM model (simulations) versus a simple Euler-Bernoulli (E-B) beam approximation is best illustrated by the examination of a simple beam structure.

Assume a free-free beam made of steel, and diameter and length of *0.2 m* and *2 m* respectively. Euler-Bernoulli beam model gives its natural frequencies as [28]

$$f_i = \frac{\lambda_i^2}{2\pi . L^2}\left(\frac{E.I}{m}\right)^{1/2} \quad ; \qquad i = 1,2,3... \tag{4.1}$$

where m is mass per unit length, and λ_i is a dimensionless parameter of the ith mode which is tabulated in Table (4.1) for free-free boundary conditions. E is 207 GPa and ρ is 7850 kg/m^3 for steel. The same beam can also be analysed by means of a FEMLAB model with the same material properties; the FEM model has 97509 DOF and 20079 second-order tetrahedral elements. Note that the beam has relatively large

aspect ratio (495/40 ≈ 12) for which one expects the Euler-Bernoulli approach to do relatively well. As the aspect ratio of the beam decreases the fundamental assumption of the Euler-Bernoulli theory must be questioned: the beam will clearly be subject to shear and the deformation will not be only in the symmetry axis of the beam. Furthermore, for aspect ratios less than 1, it will become extremely difficult to envision those objects as beams.

Table 4.1: Comparison of natural frequencies obtained by Euler-Bernoulli beam model and Femlab model for a simple free-free beam

Mode #	λ_i	**Natural Frequencies (E-B beam) (Hz)**	**Natural Frequencies (Femlab) (Hz)**	**Error (%)**
1	4,73004074	228,5652756	222,81	2,52
2	7,85320462	630,0489842	588,18	6,65
3	10,9956078	1235,147917	1091,77	11,61
4	14,1371655	2041,762266	1694,02	17,03
5	17,2787597	3050,040587	2363,57	22,51

Comparison of natural frequencies obtained by Euler-Bernoulli beam model and Femlab model can be seen in Table 4.1. Interestingly, frequencies obtained by E-B beam model are higher than the ones obtained by Femlab, and the error increases up to 23 % for the fifth mode. Main reason for this error is the assumption of E-B beam model that the shear deformation and the rotational inertia can be neglected.

4.3 Multi-Stepped Rotor

In most of the common applications, rotors are multi-stepped for the purposes of axially supporting the bearings, decreasing the rotational inertia and strengthening the critical parts of the rotor. Division of the rotor into segments as done in the proposed model allows for the proper modelling of variations such as cross sectional area, and location of bearings.

An illustration of a four-stepped (five uniform segments) rotor can be seen in Figure 4.2. This rotor is the one used in the examples in the following sections. The system dealt with in the examples has two bearing supports, and these bearings are mounted on the rotor with press-fit. Even with the interference of *5-10 μm,* the pressure between the inner rings of the bearings and the rotor reaches up to *20 MPa*. Hence, it is reasonable to assume that the inner rings of the bearing are integral to the rotor.

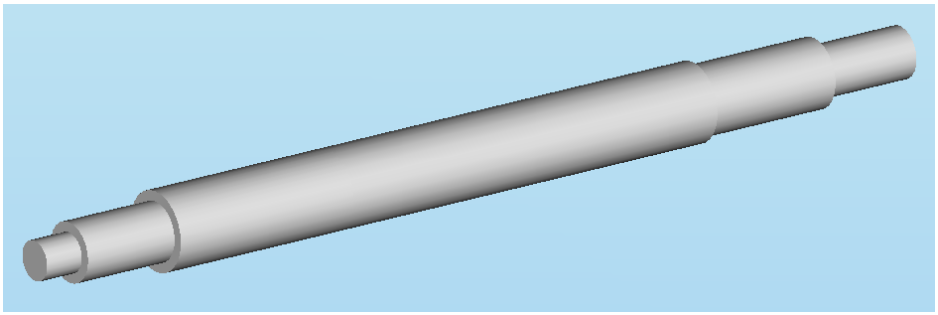

Figure 4.2: A four-stepped (five uniform segments) rotor.

With the application of the inner rings of the two bearings as added segments to the rotor, number of segments increases to seven, and the dimensions of the rotor take the form as in the following table:

Table 4.2: Dimensions of the rotor coupled with the inner rings of the bearings.

	1	**2**	**3**	**4**	**5**	**6**	**7**
L (mm)	20	70	82	375	435	445	495
D (mm)	19,8	28,5	50	40	35	42	24,5

4.3.1 Free-Free Multi-Stepped Rotor

For the analytical determination of the frequencies and the mode shapes, the effects of damping are neglected since damping is related to the time derivative of the deformation function. It is seen that with the application of arbitrary damping coefficients Femlab gives almost the same natural frequencies and mode shapes.

Without application of any constraints to the same rotor in the previous section, the frequencies obtained from the analytical and finite element models are given in Table 4.3. The error reaches up to 13 % for the fourth mode. The rate of increase in the

error seems to be similar to the case illustrated in the previous section for a simple beam. Needless to say, many sub-beams of the rotor structure hardly qualifies as beams, yet it is quite satisfactory to see the first modes are relatively close and the discrepancy in the fourth mode is not too overwhelming.

Table 4.3: Comparison of the frequencies of the analytical and finite element models for a free-free multi-stepped rotor.

Mode #	Analytical Frequency (Hz)	Femlab Frequencies (Hz)	Error (%)
1	929,7	910,6	2,05
2	2343,1	2212,5	5,57
3	4186	3782,7	9,63
4	6370,8	5514,4	13,44

The mode shapes obtained by means of the analytical model and Femlab are shown in Figures 4.3 and 4.4 respectively.

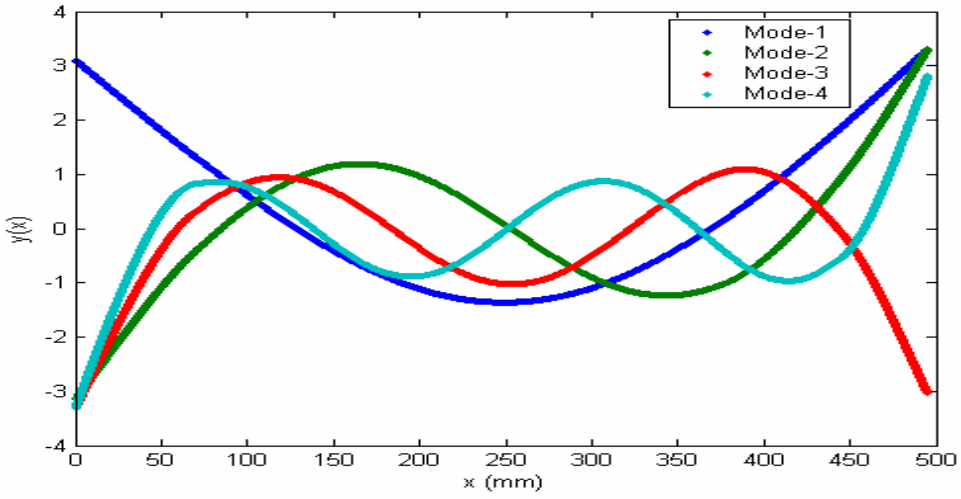

Figure 4.3: Analytically obtained mode shapes.

As it should be expected there are n peaks for the n^{th} mode of the rotor. Figure 4.3 shows the mode shapes obtained by the analytical model scaled equating the maximum values of all modes. Scales of the modes are not important as can be seen from the equations in Chapter 2 that they have no effect on the determination of the frequency response functions. What is important is the ratio between the deflections of the points

along the rotor. As can be seen in Figure 4.4, Femlab results verify the analytically obtained mode shapes.

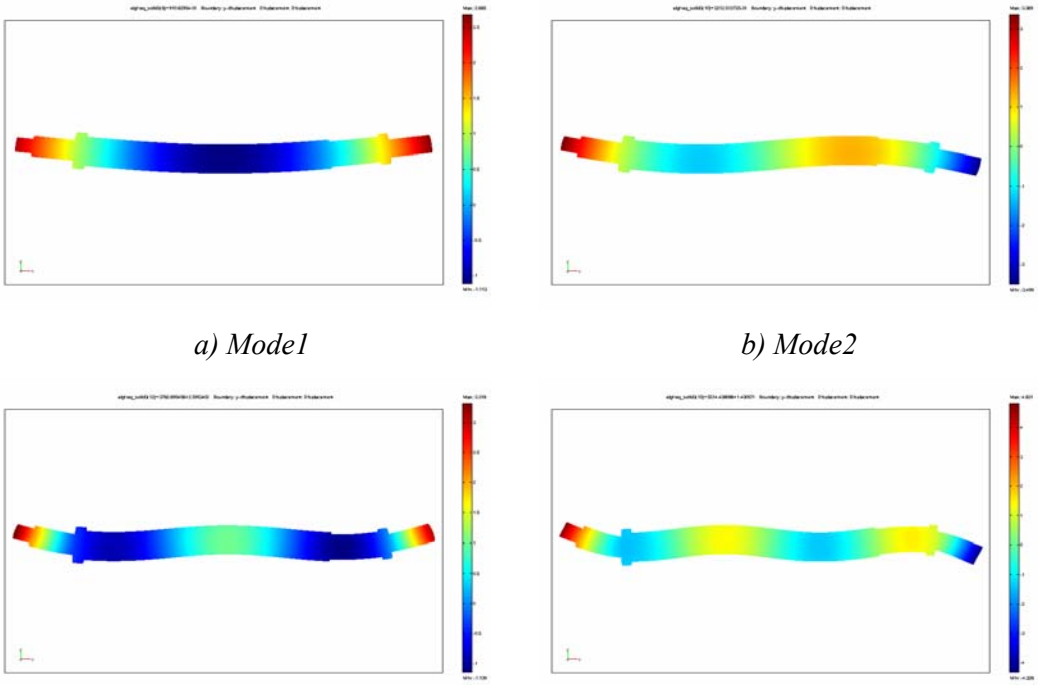

a) Mode1 *b) Mode2*

c) Mode3 *d) Mode4*

Figure 4.4: Mode shapes obtained from Femlab.

Using the frequencies and the mode shapes in the frequency response function equations given in section 2.4, one can easily get the FRFs corresponding to any excitation and response locations on the rotor. For the comparison with Femlab, it is assumed that both the excitation and response locations are the left end of the rotor. Analytical model directly gives the FRF, but to obtain the same FRF in Femlab, one must apply a force with magnitude 1 N as suggested in the manuals.

Figure 4.5 shows the undamped case for both of the models. Structures of the FRFs are similar, but there is a frequency shift which is growing for the higher modes because of the different natural frequency calculations of the analytical and Femlab models. This shift is consistent with our earlier observations that the E-B beam theory predicts higher frequencies as the mode number increases.

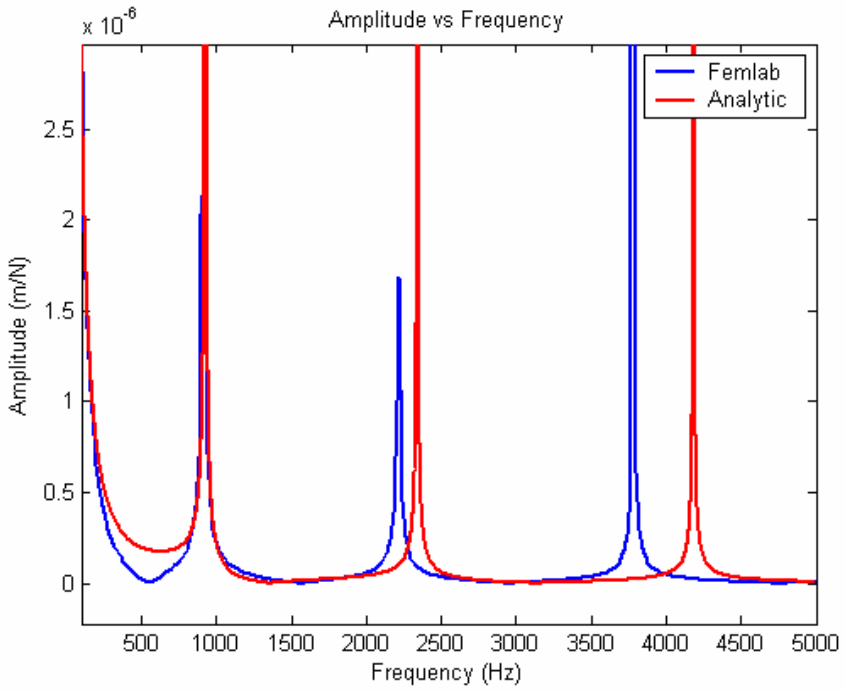

Figure 4.5: Undamped FRFs for the analytical model and Femlab.

On the other hand, Figure 4.6 shows the hysterically damped case for which the damping coefficient is kept the same for both models, *h=0,02*. Apart from the shift caused by the frequencies as in the undamped case; there are significant discrepancies between the peak values of the FRFs. Since both the analytical model and Femlab are evaluated numerically, for frequency inputs near the natural frequencies the gain is a huge number. Hence, the peak corresponding to this natural frequency seems to be higher than the other ones. On the other hand if the peak remains between any two frequency steps, the gain seems to be smaller than the actual value. The reason for this is that Matlab directly connects the consecutive data points with a smooth line in plots. That is the main reason for the differences between the peaks.

Another point worthy to mention is that Femlab uses proportional damping coefficients to model the damping, but for the modelling of the structures it is better to use hysteretic damping coefficient as explained in section 2.4.2. Although it is tried to apply the same damping coefficients for both of the cases, the structure of the equations applied in Femlab causes not to have as good results as the undamped case.

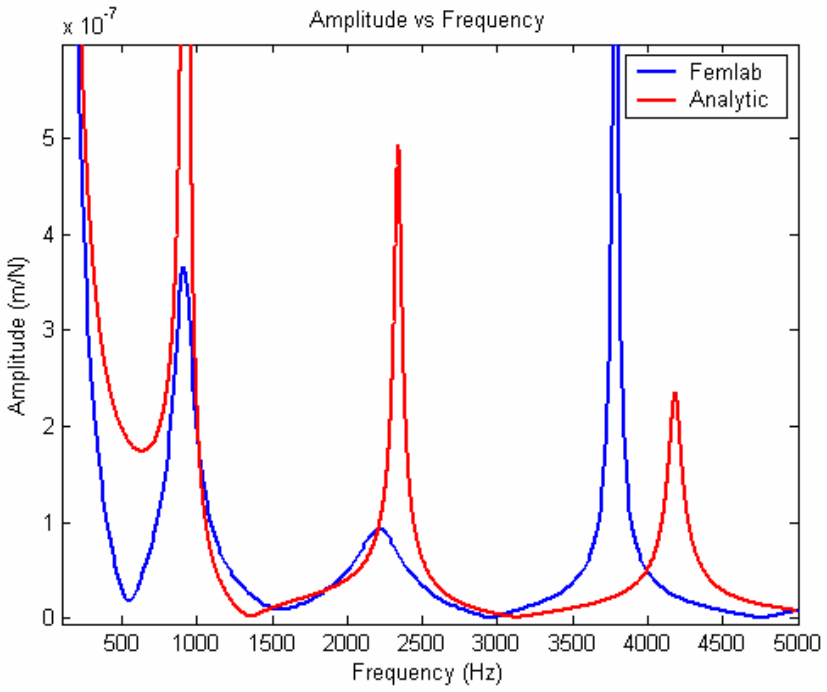

Figure 4.6: Damped FRFs for the analytical model and Femlab.

4.3.2 Pinned-Pinned Rotor

Assuming the connections between the rotor and the bearings are infinitely rigid, the system can be assumed as a rotor pinned at the bearing locations. In such a case it means that the number of the segments increase by the number of the pin supports.

Limitations due to the neglection of the rotary inertia and the shear deformation can be overcome for the case of a pinned-pinned beam. It is proposed that including just the rotary inertia to the Euler-Bernoulli beam model the natural frequencies are obtained as [29]

$$w_{n\_r}^2 = \frac{w_n^2}{1+(n^2.\pi^2.r^2)/l^2} \tag{4.2}$$

where w_n is the natural frequency obtained by E-B beam model, n is the mode number, l is the distance between the supports and r^2 is

$$r^2 = \frac{I}{A} \tag{4.3}$$

with I being the area moment of inertia.

The natural frequencies neglecting the rotary inertia, but including the shear deformation can be obtained by means of Timoshenko beam model as [29]

$$w_{n\_s}^2 = \frac{w_n^2}{1+\left((n^2.\pi^2.r^2)/l^2\right)\left(E/\kappa.G\right)} \tag{4.4}$$

where G is the shear modulus, and κ is Timoshenko's shear coefficient and given for cylindrical beams as

$$\kappa = \left(6+12.\nu+6.\nu^2\right)\left(7+12.\nu+4.\nu^2\right) \tag{4.5}$$

with ν being the Poisson's ratio.

Assume that the bearing locations for the illustrated rotor are 76 and 440 mm from the left end. Applying these conditions to the analytical model and Femlab, one can obtain the frequencies as in the Table 4.4. The results show that the addition of rotary inertia improves the model better than the addition of the shear deformation. Since the illustrated rotor can be assumed as slender (aspect ratio > 10), shear deformation does not have as strong effect as the rotary inertia. Thus one can say that it is more logical to use the frequencies obtained with the addition of rotary inertia for the calculation of the frequency response functions of a slender rotor.

Table 4.4: Comparisons of the frequencies obtained from the revised analytical models with FEM frequencies for a pinned-pinned multi-stepped rotor.

Mode #	**Femlab (Hz)**	w_n **(E-B) (Hz)**	**Error with Femlab(%)**	w_{n_r} **(Hz)**	**Error with Femlab(%)**	w_{n_s} **(Hz)**	**Error with Femlab(%)**
1	585,3	594,9	1,6	592,7	1,3	594,9	1,6
2	2094,8	2208,5	5,4	2176,6	3,9	2207,7	5,4
3	3520,9	3978,8	13	3851,8	9,4	3975,6	12,9
4	4440,6	5234,4	17,9	4947,9	11,4	5226,8	17,7

Mode shapes of the analytical model can be seen in the Figure 4.7. The locations of the supports which should be remained fixed are obvious.

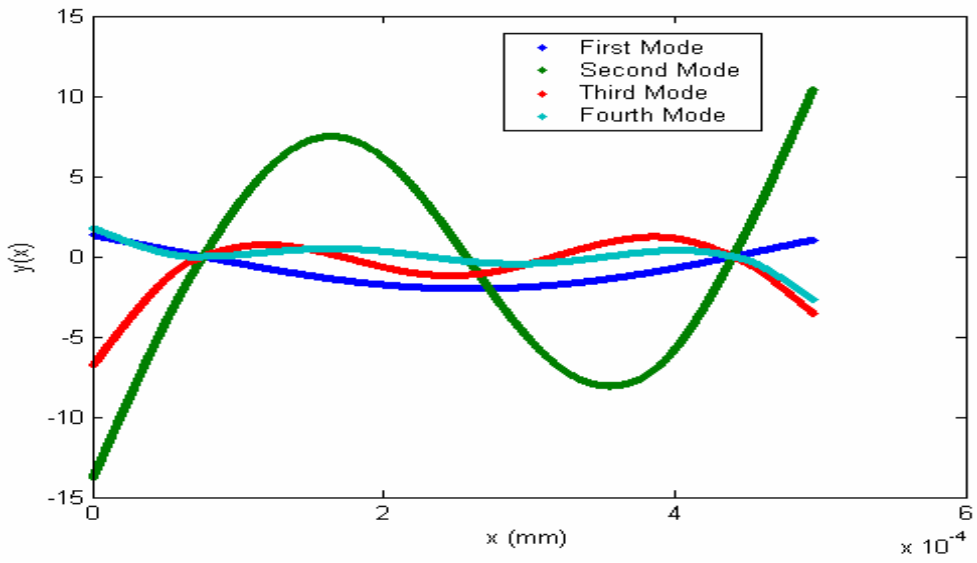

Figure 4.7: Analytically obtained mode shapes.

As can be seen in Figure 4.8, Femlab results verify the analytically obtained mode shapes with the same number of peaks and similar structures.

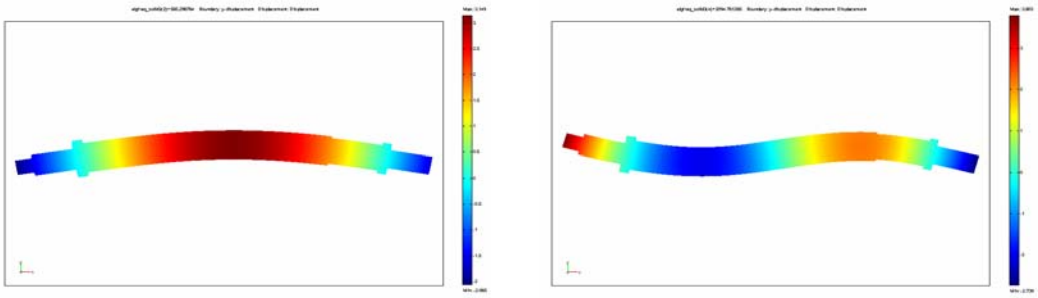

a) Mode1

b) Mode2

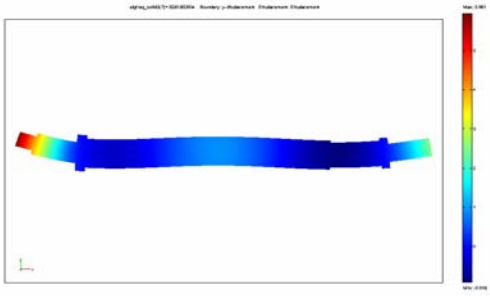

c) Mode3

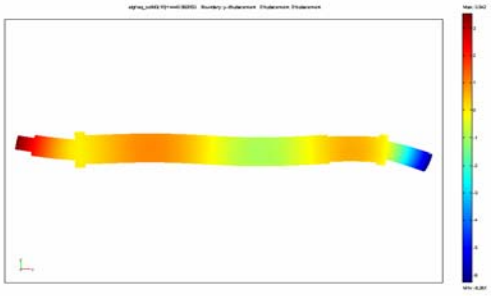

d) Mode4

Figure 4.8: Mode shapes obtained from Femlab.

For the undamped case FRFs are very similar and the frequency shift is less with the application of rotary inertia as can be seen in the Figure 4.9.

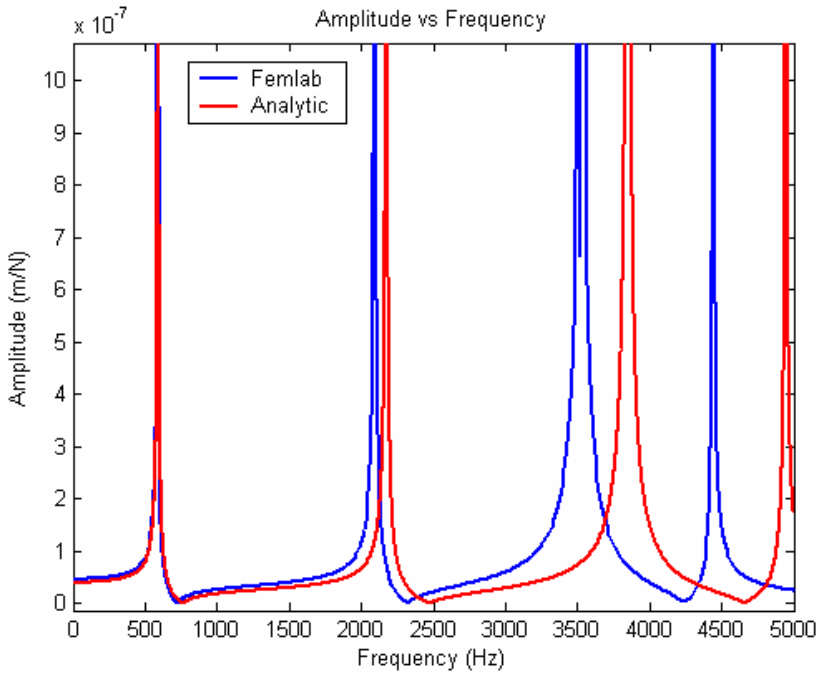

Figure 4.9: Undamped FRFs for the analytical model and Femlab.

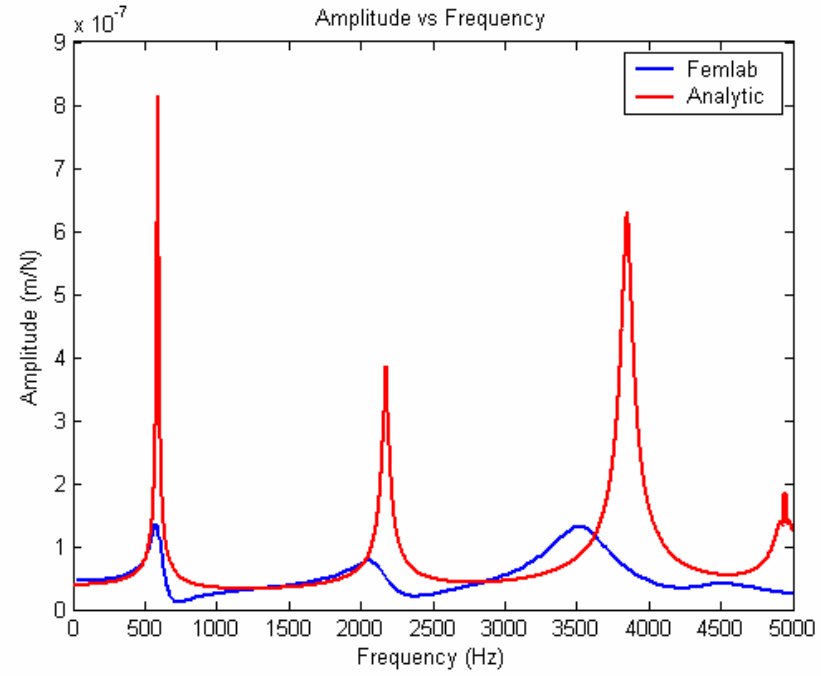

Figure 4.10: Damped FRFs for the analytical model and Femlab.

Application of the same hysterical damping coefficients; *h=0,02*; for both of the models gives the result as seen in Figure 4.10. Inclusion of the effect of the rotary inertia help decrease the shift in the natural frequency for higher mode numbers, but similar to the free-free beam studied in the previous section, FRFs do not fit each other so much for two models because of the unresolved peaks, and the 3D vs 2D effects.

4.4 Contact and Bearing Stiffness

The effective stiffness of a rotor-bearing system is determined not only by stiffness characteristics of the rotor but also by the interactions between the rotor and the supports. With the assumption of rigid connection components, these interactions only consist of the contact parameters. These contact parameters can have important influence on the dynamics of the rotor-bearing systems.

For the case of a bearing mounted between a shaft and housing, there are mainly two different types of stiffness. First is the cylindrical connection stiffness at the interface of the races of the bearing with the shaft and the housings. Second is the stiffness between the rollers and the races of the bearings, namely the stiffness of the bearing.

In this section, the model proposed in Chapter 3 is implemented to determine the connection stiffness. For the implementation of the model, the specifications of the experimental set-up described in the next chapter are used since some experimental data is also needed.

First it is assumed that the inner races of the bearings are integral to the shaft because of the press-fit connection in-between. Then the stiffness between the outer race and the housing is determined as explained in section 3.1. Some of the required data of the experimental set-up are as follows: The clearance is about 30 μm. The linear contact compliance is 0,3 μm/MPa for the steel/cast iron pair with about 30 μm clearance. The nonlinear contact compliance is taken as 0,7 $\mu m/MPa^{0,5}$ for fine turning [24].

For the interactions between the bearings and the housings of the experimental set-up, force/deformation relation of the linear and nonlinear models for the cylindrical connections with clearance fit can be seen in Figure 4.11. In order to cause a

deformation of only 2 μm, bearing with 35 mm inner diameter must be loaded up to 1,2 kN; and for the bearing with 40 mm diameter it is about 1,6 kN. By means of the figures one can assume constant stiffness values for the low load application; and so the stiffness values for the contacts can be estimated as Kh_35=582e6 N/m and Kh_40=787,5e6 N/m.

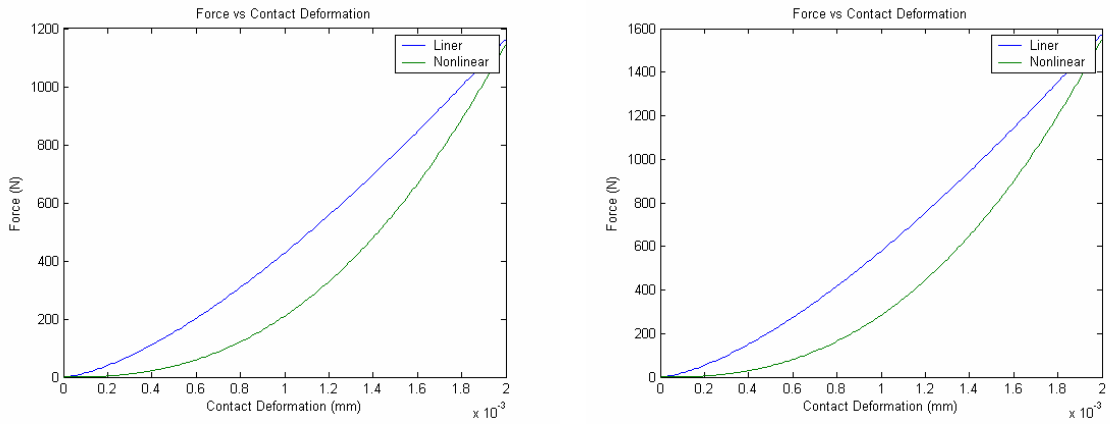

a) Bearing_35 *b) Bearing_40*

Figure 4.11: Force-deformation relations of the clearance fit contacts.

In order to determine the bearing stiffness, the models in the sections 3.2.2 and 3.3 are applied. Since the balls have two contact surfaces, one with the inner race and one with the outer race, the contact stiffness model should be applied two times for a single bearing.

Determination of the stiffness of the bearing consists of a several steps. First, one should find the friction coefficients between the housings and the outer races of the bearings. It is assumed that applied preloads for both of the bearings are equal, which is usually the case. This results in the equality of the friction coefficients at both of the housings as explained in section 3.3.

The stiffness of bearing is dependent on the applied radial load. Since this radial load can be written in terms of the friction coefficient as mentioned in section 3.3, so the stiffness of the bearing can also. Moreover, the total stiffness at any of the housings is the resultant stiffness of the two serially connected springs corresponding to the stiffness of the bearing and the clearance fit between the housing and bearing. Thus, since the stiffness of the clearance fit can be determined as explained above, the total stiffness of the housing must also be written in terms of the friction coefficient.

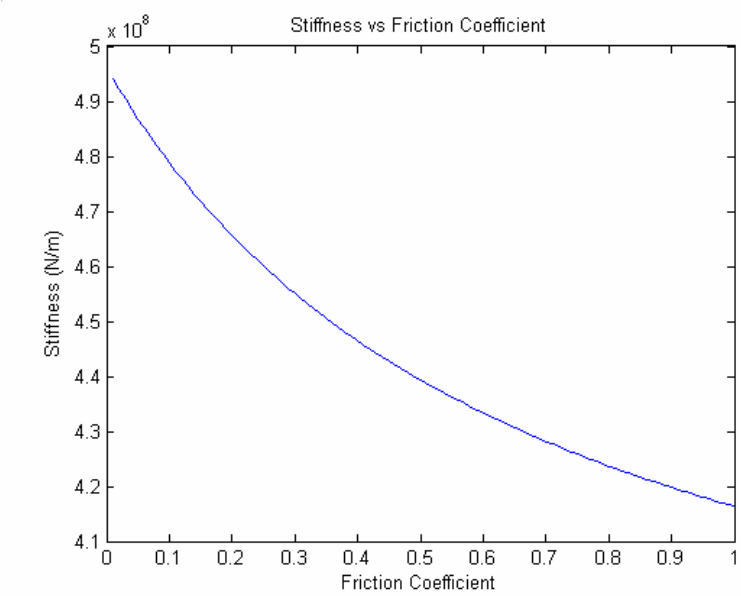

Figure 4.12: Total stiffness of the housing with bearing_35 vs the friction coefficient.

For the purpose of illustration, total stiffness of the housing of 35 mm bearing is plotted by means of a Matlab® code in Figure 4.12, for which the preload is 600 N and the external load of 900 N is applied at the tip of the shaft. As the friction coefficient increases stiffness decreases monotonically as seen in Figure 4.12.

Using this relation between the friction coefficient and the total stiffness at one housing, the method explained at end of the section 3.3 is applied for the determination of the friction coefficient and the total stiffness.

Deformation of the shaft with rigid pinned-pinned supports is determined by means of Femlab for different loads and is shown in Table 4.5 for the tip of the shaft. Subtracting these values from the experimentally obtained deformations of the shaft, bearings and housing system given in section 5.2, remaining deflection values are the ones caused by the deformation of the supports.

Table 4.5: Pinned-pinned shaft deflection values in Femlab.

Load (N)	300	600	900
Deflection (µm)	11,89	23,75	35,66

Knowing the total stiffness of the housings in terms of the friction coefficient, one can implement a simple algorithm to relate the deflection caused by the deformations of

the supports with the friction coefficient, and then to obtain the corresponding friction coefficient value. For an illustration, the case of 200 N preload and 300 N external load is shown in the Figure 4.13. The friction coefficient value for the deflection of 3,61 μm is about 0,2625.

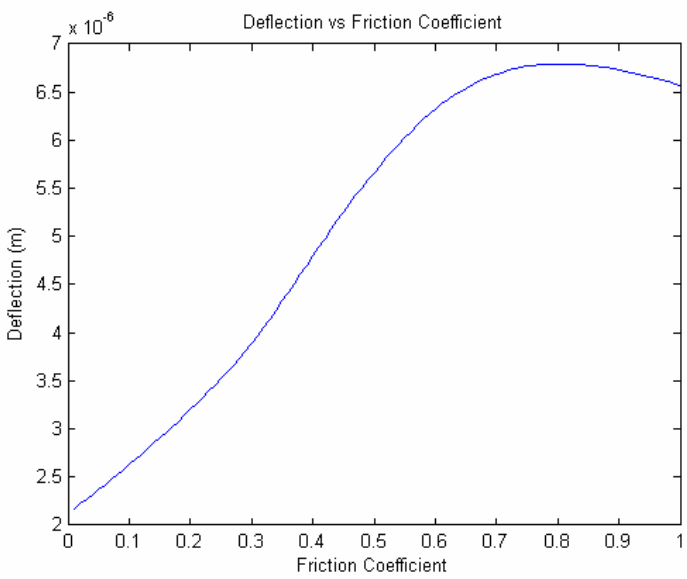

Figure 4.13: Deflection vs friction coefficient.

For different values of preloads and external loads, the obtained friction coefficients are shown in Table 4.6. It can be concluded that external force has not so much effect on the friction coefficient; and friction coefficient reaches its maximum value of '1' between the preloads of 400 and 600 N.

Table 4.6: Friction coefficients under different conditions.

	Preload (N)		
External Force (N)	**200**	**400**	**600**
300	0,2625	0,7929	>1
600	0,2439	0,7558	>1
900	0,2601	0,7282	>1

In the FAG Super Precision Bearings catalogue [30], the radial stiffness of the bearings for low, medium and high preloads are supplied. For the bearings used in the experimental set-up, these values are shown in Table 4.7. The corresponding friction

coefficients for bearings that are calculated by the method described above are also listed in a separate column in the table.

Table 4.7:Stiffness and friction coefficients of the bearings depending on the preload.

Bearing_35			Bearing_40		
Preload (N)	**Stiffness (N/m)**	**Fric. Coeff.**	**Preload (N)**	**Stiffness (N/m)**	**Fric. Coeff.**
61	2,178e8	0,0274	85	2,466e8	0,068
209	3,846e8	0,3093	300	4,374e8	0,475
481	5,958e8	0,5901	633	6,444e8	0,8141

The friction coefficients obtained by means of the model and the experimental data are plotted with these catalogue values in Figure 4.14.

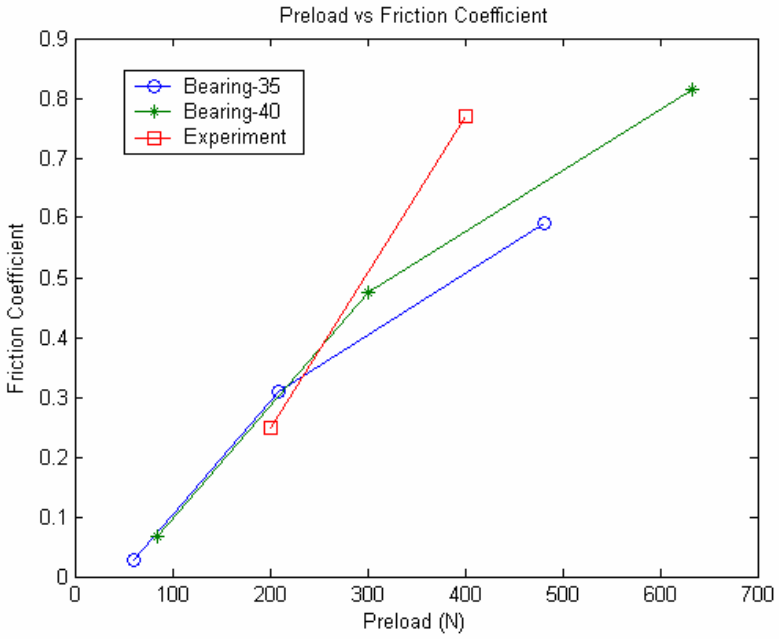

Figure 4.14: Comparison of the friction coefficients.

In conclusion, one can claim that the friction coefficient is only a function of the preload for the same type of bearings. Thus with the help of precise experimental data for a bearing, the proposed model can estimate the stiffness of any bearing, that belongs to the same group for any preload and external load.

4.5 Rotor-Bearing Systems

Rotor-bearing systems can simply be modelled as a rotor supported by the springs and dampers. Since both the rotor model and the connection stiffness model are developed in the previous sections, coupling of these models results in a simple model of the rotor bearing system.

Applying the stiffness values obtained for the bearing and housing assembly to the rotor at the support locations in both the analytical and finite element models, the natural frequencies are obtained as follows:

Table 4.8: Comparison of the frequencies of the analytical and finite element models for a rotor-bearing system.

Mode #	Analytical Frequency (Hz)	Femlab Frequencies (Hz)	Error (%)
1	590,6	574,2	2,78
2	2114,7	2025,3	4,23
3	3729,1	2889,7	22,51

First two frequencies are close to each other, but for the third natural frequency the error is huge. This is mainly because of the application of the spring force to a single point in the 3-D Femlab model. Although this holds for the analytical model, since each point corresponds to a cross sectional plane, spring force acts on the whole plane.

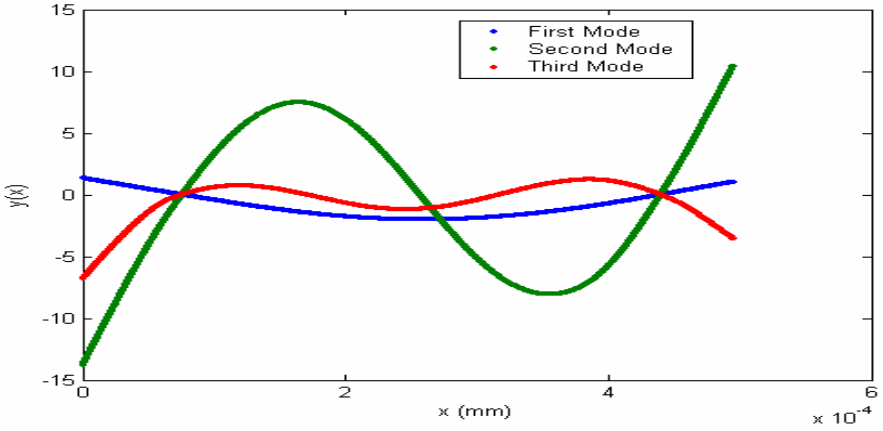

Figure 4.15: Analytically obtained mode shapes.

Mode shapes of the analytical model can be seen in Figure 4.15. The locations of the spring supports are obvious because of their high stiffness. As can be seen in Figure 4.16, Femlab results verify the analytically obtained mode shapes with the same number of peaks and similar structures.

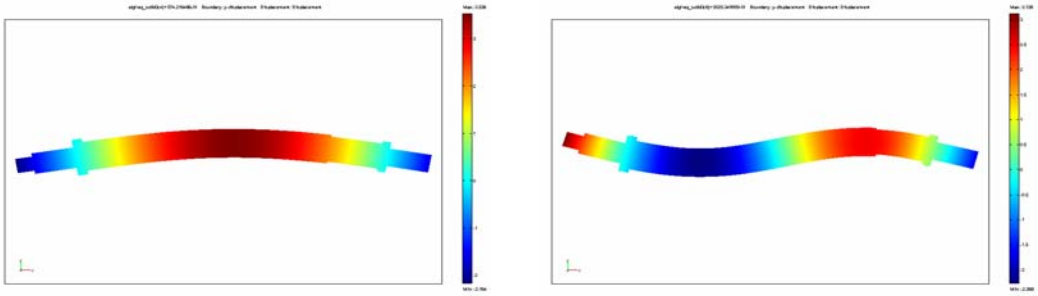

a) Mode1 *b) Mode2*

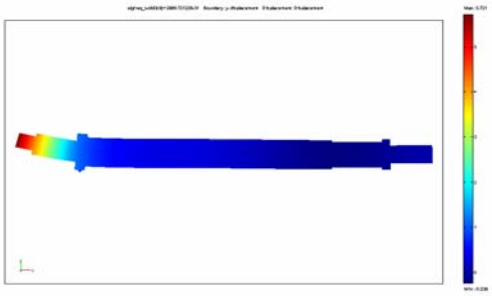

c) Mode3

Figure 4.16: Mode shapes obtained from Femlab.

FRF of the rotor-bearing system for the undamped case is shown in the Figure 4.17. The frequency shift of the third mode is much more with respect to first two ones which is because of the discrepancy of the third mode frequencies between the EB model and the FEMLAB Moreover, FRFs are very similar qualitatively, and fit well for the first mode, and somewhat well for the second mode.

Application of the same hysterical damping coefficients; $h=0,02$; for both of the models gives the result as seen in Figure 4.18. Difference between the FRF structures comes from the damping model of Femlab, and the same frequency shift problem is valid.

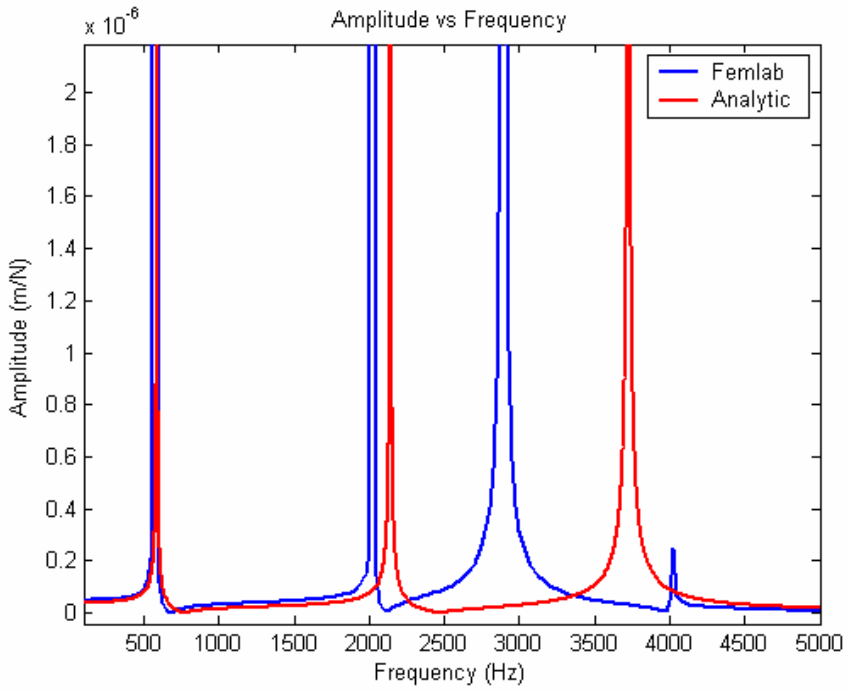

Figure 4.17: Undamped FRFs for the analytical model and Femlab.

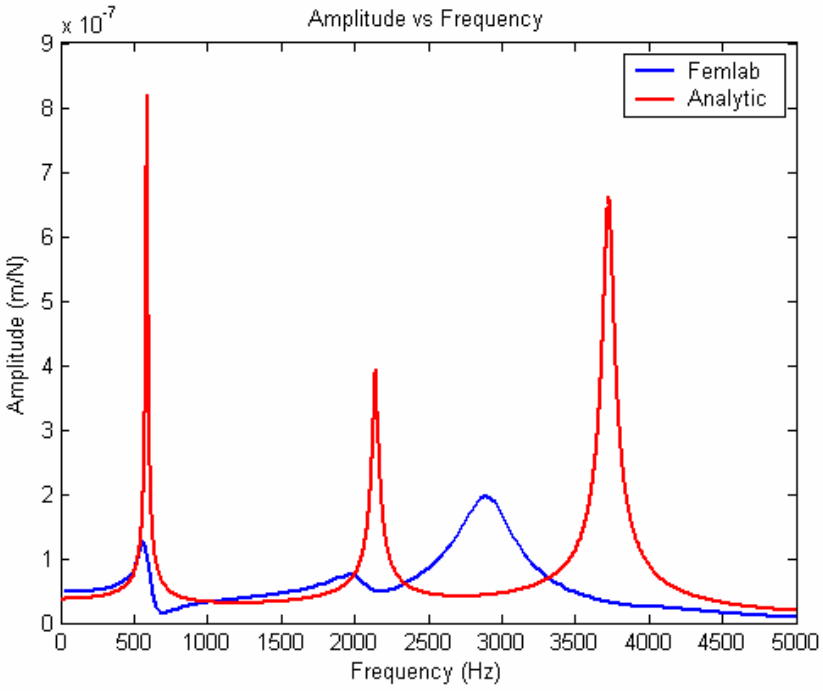

Figure 4.18: Damped FRFs for the analytical model and Femlab.

5 EXPERIMENTAL SET-UP AND RESULTS

This chapter presents the experimental set-up manufactured for the tests to be used in the verification of analytical models and the identification of some parameters. The methods and experimental tools used for the tests are also discussed in detail. Finally the application of a method for the coupling of substructures to the experimental set-up is explained, and obtained results are discussed.

5.1 Experimental Set-up Design and Specifications

In modern machine tool systems, high speed spindles are frequently used to provide high speed machining capability. High speed spindles are the most critical elements of high speed machine tools and usually very expensive.

The objective of the preparation of such an experimental set-up was to obtain a spindle-bearing system similar to the spindles of high speed machining applications. The major components required for a spindle-bearing system include:

- Spindle Shaft
- Spindle Bearings
- Spindle Housing
- Spindle Motor

Since the flexural vibration of the rotor is under consideration with the assumption that the natural frequencies are independent of the rotational speed, there is no need for a drive motor in the test set-up.

The spindle shaft is quite important because it transfers the power from the motor to the cutting tool in a HSM application. The shaft must locate and support the bearings. One important design consideration for the shaft is bending. During a high speed operation, the shaft will exhibit bending deformations. The frequency at which the shaft

will bend depends on the diameter and length of the spindle shaft. It is often tempting to design a long spindle shaft, as this allows for a more powerful motor for the spindles with integral motors. However, care must be taken as the spindle grows in length, the bending modes will be very flexible. This is not tolerable for a spindle, and must be resolved by either re-designing the shaft with a larger diameter- in which case the bearings will be larger and the maximum allowable speed will be lower- or decreasing the shaft length.

The shaft usually contains the complete tooling system but for the sake of simplicity a solid shaft without any internal diameter is chosen. The main reason is the manufacturing cost of a hollow shaft with good tolerance integrity. This however does not impose an important limitation in testing and modelling as only the moment of inertia would be affected due a hollow shaft which can easily be calculated. The dimensions of the shaft determined using similar aspect ratios of the segments with the spindles of GMN [2]. The shaft chosen is as shown in Figure 4.2 and its dimensional properties are in Table 5.1.

Table 5.1:Dimensions of the shaft .

	1	**2**	**3**	**4**	**5**
L (mm)	20	70	375	445	495
D (mm)	19,8	28,5	40	35	24,5

Another very critical component of a high speed spindle is the bearing system. The spindle must provide high rotational speed, transfer torque and power to the cutting tool, and be capable of withstanding the loading with reasonable life. The bearing type used must be consistent with these demands, or the spindle will not perform properly.

High precision bearings are available today from a variety of manufacturers worldwide. The types of bearings available for high speed spindles include roller, tapered roller and angular contact ball bearings. Each bearing type has its own advantages. A spindle that is desired to have the highest speed will not have the maximum stiffness possible, and the spindle with the highest stiffness cannot run at high speeds without sacrificing bearing life.

Angular contact bearings are most commonly used today in very high speed spindle designs. This is due to the fact that angular contact ball bearings provide the

precision, load carrying capacity and speed required for metal cutting spindles. In some cases, tapered roller bearings are used, due to their higher load capacity and greater stiffness over ball bearings. However, tapered roller bearings do not allow the high speeds required by many spindles.

Angular contact ball bearings utilize a number of precision balls fitted into a precision steel race. They are designed to provide both axial and radial load carrying capacity, when properly pre-loaded.

In order to provide the required load carrying capacity for a metal cutting machine tool spindle, several angular contact ball bearings are used together. This way, the bearings can share the applied loads, and increase the overall spindle stiffness. The bearings can be installed several ways, depending upon the desired characteristics. In many cases, two or three bearings are placed near the spindle nose, with a pair mounted near the rear of the spindle shaft. The most common technique used is back to back configuration as shown in Figure 5.1. This configuration is suited for most applications and provides good accuracy and rigidity.

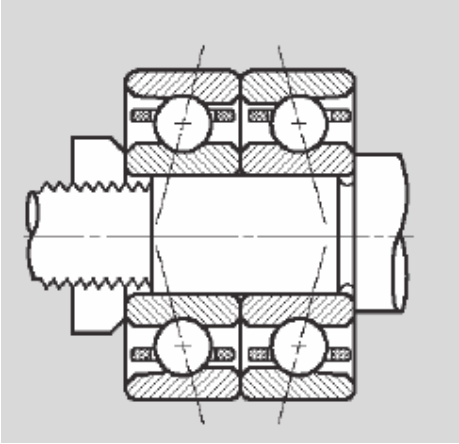

Figure 5.1: Back to back configuration.

Angular contact ball bearings must be pre-loaded in order to provide axial and radial load carrying capabilities. One simple way to do this is to mount the bearings in groups of two or three, such that the pre-load is correctly applied to the bearings. The inner or outer bearing races are ground, such that when clamped together the bearings will have the proper amount of pre-load. Springs are usually used to provide a pre-loading force against the spindle shaft in the axial direction. Different types of this preloading are shown in Figure 5.2. For the spindle system developed, angular contact

ball bearings in back-to-back configuration with spring preload are used. Specifications of the bearings used are as in Table 5.2.

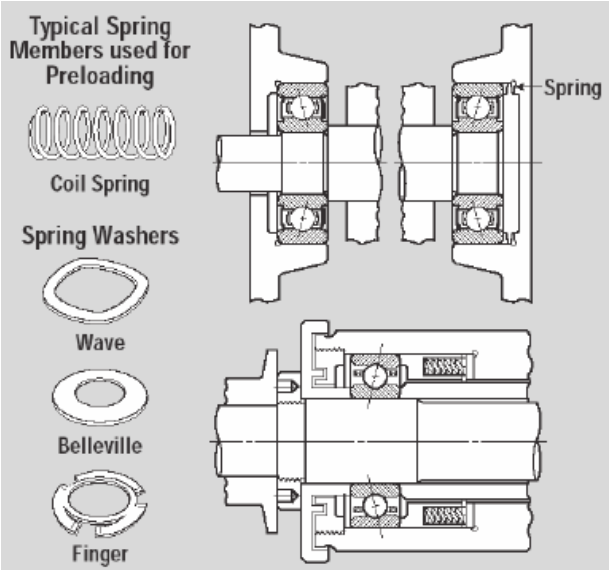

Figure 5.2: Different types of spring preloading [31].

Table 5.2: Bearing specifications.

Bearing Code	Inner Dia.(mm)	Outer Dia.(mm)	Width (mm)	Ball dia. (mm)	Contact Angle	# of balls
B71907C.T.P4S	35	55	10	6,35	15^{o}	17
B71908C.T.P4S	40	62	12	7,14	15^{o}	18

The spindle shaft must be held in housing. The primary function of a spindle housing is to locate the bearings. The spindle housing must support and locate the bearings accurately, and provide the utilities needed by the spindle system. It must be robust and stiff, as the housing transfers all forces from the spindle to the machine tool. High precision bearings must be positioned exactly in terms of geometry and size. For these reasons, housings and base were chosen as rigid and heavy as possible.

Figure 5.3 shows the spindle system constructed. Since it is also desired to change the bearing locations to find their optimum locations for different conditions, the housings are mounted on the base in a way that they can slide through the axes of the shaft by means of the sledge. During the experiments housings can be rigidly connected to the base with the bolt and nut system as shown.

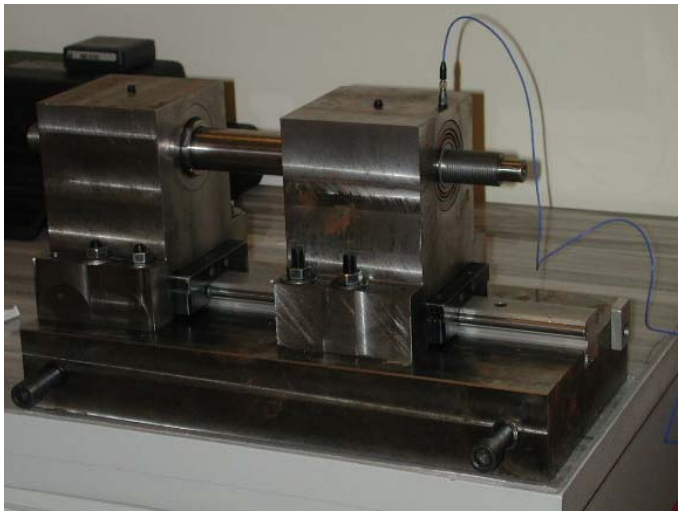

Figure 5.3: Experimental set-up.

Figure 1.4 shows the CAD drawing of the experimental set-up with its inside details. The preload springs do not contact the shaft since their inner diameters are bigger than the corresponding segment diameters. Compression of the springs is achieved by the nuts which have thread connections to the holes of the housings. Thus, the bearings are preloaded by tightening the spring nuts. Spring forces corresponding to the amount of compression were tabulated before they are mounted onto the system, by deforming them by means of a hydraulic press and measuring the spring force.

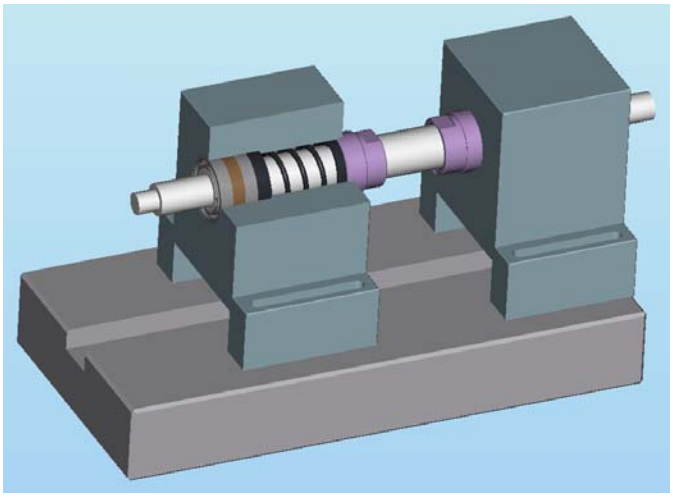

Figure 5.4: CAD drawing of the experimental set-up showing inside details.

In Figure 5.4, the spacer between the bearings can also be seen with brown colour. The pre-load is applied by the spring to the first bearing, and by means of this spacer the

second bearing is also pre-loaded with the same amount. Thus the proper distribution of the preload on each of the bearings is achieved.

5.2 Static Deflection Test

For the method described in section 3.3 and implemented in section 4.4, the static deflection values of the shaft in the experimental set-up are needed. This was accomplished by placing the experimental set-up in a hydraulic press as shown in Figure 5.5. Different forces applied to the tip of the shaft under different preload conditions and the deflection of the tip measured by means of a digital dial gage. A digital dynamometer was placed between the tip of the hydraulic press and the shaft to measure the applied force.

Figure 5.5: Static deflection test.

When the load is applied by the press, the whole set-up may move in the level of microns and may cause incorrect measurements. In order to avoid this, the dial gage must be placed on the base or better on the housing to measure the relative deflection between the shaft and the housing.

Digital dial gage has a 1μm resolution which is not ideal for such small deflections. Thus, for the purpose of obtaining more precise results, measurements performed many times for the same conditions, and the average values are tabulated as in Table 5.3.

Table 5.3: Deflection measurements of the shaft.

	Preload (N)		
External Force (N)	**200**	**400**	**600**
300	14	14	15,2
600	30,3	31	32,75
900	46,3	48	49,25

One can conclude from Table 5.3 that under the same external force conditions, deflection of the shaft increases as the preload increases. This means that under same conditions, increase in preload causes decrease in stiffness. This unexpected result is perhaps because of the lack of precise measurement conditions. But one can also make a reasonable explanation of this situation that the increase in preload does not always result in increase in stiffness. Under some external load and preload conditions not all of the balls share the radial load. In such a case, as preload is increased, the number of balls sharing the radial load increases. This lowers the individual contact load and thereby decreases stiffness. Eventually, a preload level will be reached that will create a 100% load zone, thereby creating an increase in stiffness with further preloading. Experiment results show that this preload level was not reached for these specific cases and an increase in preload causes decrease in stiffness.

5.3 Dynamic Impact Test

Modal analysis is widely used in the experiments to obtain vibration characteristics of machine structures. Complete dynamic description of a machine requires the determination of modal frequencies, mode shapes and system parameters (equivalent mass, stiffness and damping ratio). Experimental modal analysis deals with a method of measuring the response of a machine, structure or system to an excitation

and using this information identifies some of its dynamic properties. The response of a system can be measured in terms of its displacement, velocity, or acceleration.

Frequency response function plays an important role in the experimental modal analysis. The FRFs are first determined experimentally and then analyzed to find the natural frequencies, mode shapes and system parameters. The system parameters (equivalent mass, stiffness and damping ratio) can be used to predict the response of the system to various excitations.

General arrangement for the frequency response measurement of the experimental set-up is shown in Figure 5.6. FRF measurement is performed with impact hammer tests. A hammer is used to apply an impact load at different points of the system while an accelerometer is fixed at one location to measure the response. It is very important to choose the correct type of hammer or accelerometer to be used. For the measurements of structures with high mass like housings, a bigger hammer and an accelerometer with higher sensitivity must be used to obtain reliable results. A simple PC or laptop can be used to collect the data, estimate the modal parameters and display the results.

Figure 5.6: FRF measurement system.

The hammer consists of an integral, quartz force sensor mounted on the striking end of its head. The impact force is transferred into electrical signal for display and analysis. These sensors are easy to operate and interface with signal conditioning, data acquisition and recording instruments.

Time response of the accelerometer is measured and converted into frequency domain. Fast Fourier Transform (FFT) is used to convert the time data. The white box seen in the figure is the I/O box with two high accuracy filters in. It is connected to the laptop with a data acquisition card.

For the analysis of the system in the laptop, a program named CUTPRO® [32] is used. MALTF®, which is a module of CUTPRO® [32], is a special software for the measurement of frequency response functions of structures. CUTPRO® has its own modal analysis software as well. Using the transfer function measurements, it determines the dynamic parameters of a system.

For the verification of the models described in previous chapters, many tests were performed on the set-up. The simplest comparison can be made for the free-free shaft between the experimental and analytical results. Figure 5.7 shows the shaft hanged with cords.

Figure 5.7:Free-free shaft hanged with cords.

The shaft excited with the impact hammer and the response measured with the accelerometer in the lateral direction. The reason is that in the vertical direction tensions in the cords would create a support, thus it would no more be a free-free shaft. It is also expected that the rigid body modes of the shaft would not be sensed by the accelerometer properly. Rigid body modes have zero natural frequencies which are out of the measuring range of the accelerometers.

For the analytical determination of the FRFs of the shaft, the hysteretic damping ratio coefficient is taken as 0,001 which is obtained from the modal analysis module of CUTPRO®. This damping ratio is taken as the average value of the first three modes.

Figure 5.8 shows the direct FRFs obtained analytically and experimentally at the tip of the shaft meaning that both the force and response locations are at the tip. The difference in between the prediction and the measurement till 700 Hz is because of the rigid body modes as explained. Again, a frequency shift problem exists here as in the case of comparison with FEM, which has the origin of Euler-Bernoulli beam model assumptions. But disregarding the frequency shift, it can be said that the agreement is reasonable.

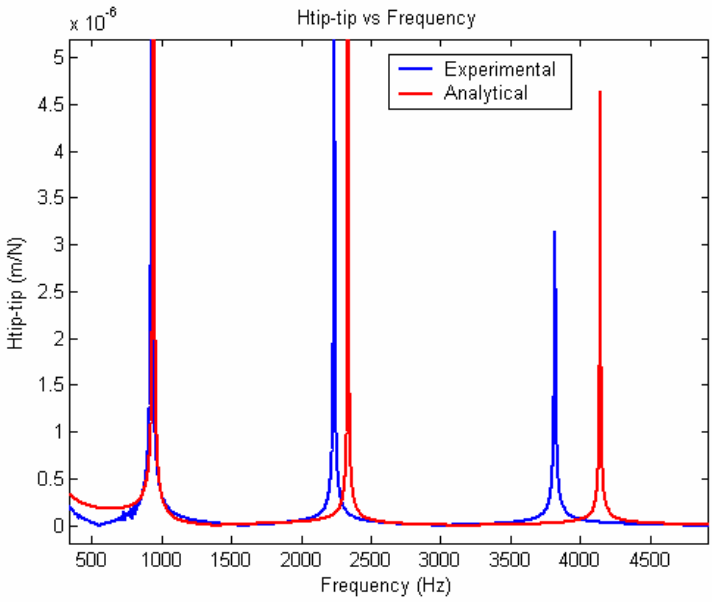

Figure 5.8: FRFs of the tip of the shaft.

FRFs obtained at the mid of the shaft which is the location of the bearing with 40 mm diameter is shown in Figure 5.9. Same comments are valid also for this case. One important remark is that the third mode which corresponds to a mode shape where the the shaft tip bends the most as shown in Figure 4.4 has nearly no effect for this bearing location as obtained from both analytical and experimental methods.

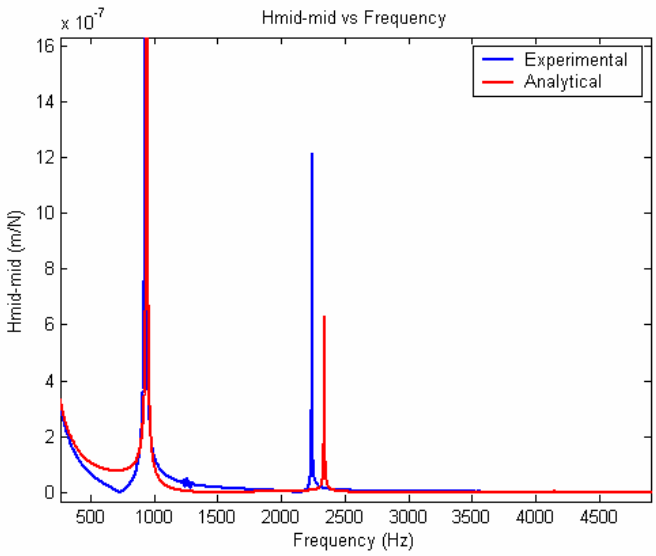

Figure 5.9: FRFs of the mid of the shaft.

One can conclude from Equations (2.56 and 67) that the cross FRFs corresponding to any two points should be same no matter which one is the excitation or the response point. This means that FRF of point-1 with respect to point-2 should be the same for FRF of point-2 with respect to point-1. Figure 5.10 shows the comparison of the experimental FRFs of two interchanged points and the analytical FRF. Experimental FRFs fit each other very well, and the difference with the analytical FRF has the same reasons as explained before.

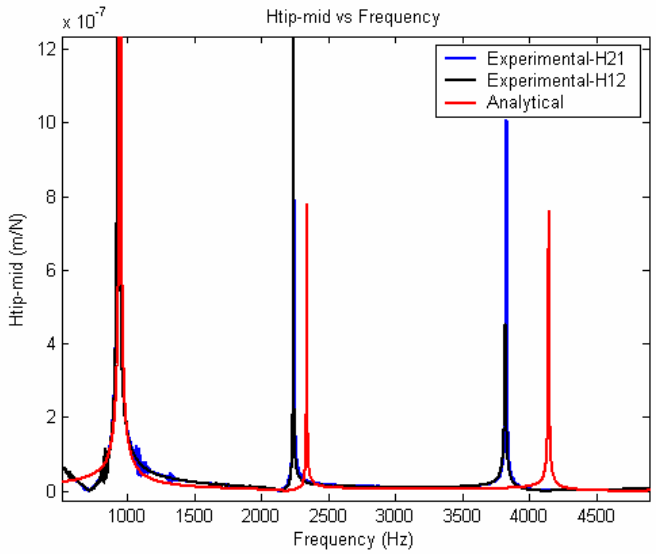

Figure 5.10: FRFs of the shaft for tip-mid couple corresponding for force an response.

These three comparisons verify the analytical model with the dynamic experiments. Existence of the same frequency shift problem means that the E-B beam model overestimates the frequencies increasingly with the higher modes.

5.4 Receptance Coupling

The theoretical analysis of a large structure can often be made much more efficiently if it is broken down into its component parts. Then, each sub-structure can be analyzed individually using the most appropriate analysis method, and such representations can be combined together via a procedure called *coupling* or *sub-structuring*.

Several coupling algorithms are well established for combining the dynamics of substructures. These methodologies provide an efficient synthesis of total structural dynamics from the analytical, finite element and experimental results of its substructures. In this section receptance coupling technique is applied on the experimental set-up.

The experimental set-up is divided into two sub-structures: the shaft and the all of the remaining parts including the housing, base and the table, etc… For the purpose of determination of the connection parameters between the shaft and the housing, the FRF of the whole structure should be equated to the coupled sub-structures with these parameters in between. FRFs of the total structure and the shaft are measured as shown in Figures 5.6 and 5.7, respectively. One must also measure the FRFs of the second sub-structure (housings, base, etc…). This is done as shown in Figure 5.11 with the use of big hammer since it is a massy structure.

Figure 5.11: FRF measurement of the second sub-structure.

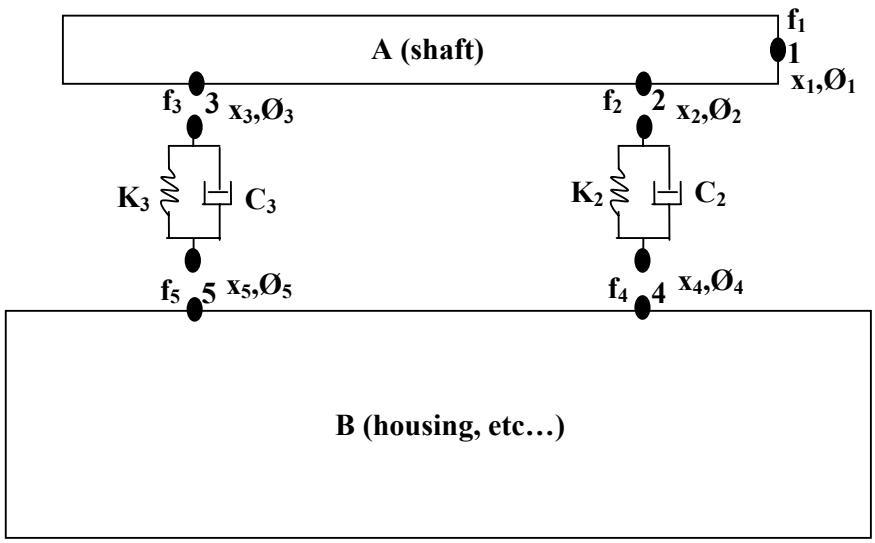

Figure 5.12: Receptance coupling process of the experimental set-up.

The application of the receptance coupling to the experimental set-up is shown in Figure 5.12. It is assumed that there is no moment applied at the bearing locations to the shaft which is a reasonable assumption for the type of the bearings used. The torsional stiffness and damping of the connections are also assumed as negligibly small.

For the free-free shaft A which is in response to virtual force at point-1, the receptance matrix is as follows

$$A_{mn} = \begin{bmatrix} D_{mn} \\ S_{mn} \end{bmatrix} \tag{5.1}$$

where D_{mn} relates the deflection at m to virtual force at n, and S_{mn} relates the slope at m to virtual force at n.

Then, the responses of the coordinates to virtual forces

$$\begin{pmatrix} x_1 \\ \theta_1 \end{pmatrix} = A_{11}.f_1 + A_{12}.f_2 + A_{13}.f_3 \tag{5.2}$$

$$\begin{pmatrix} x_2 \\ \theta_2 \end{pmatrix} = A_{21}.f_1 + A_{22}.f_2 + A_{23}.f_3 \tag{5.3}$$

$$\begin{pmatrix} x_3 \\ \theta_3 \end{pmatrix} = A_{31}.f_1 + A_{32}.f_2 + A_{33}.f_3 \tag{5.4}$$

For the sub-system B, similarly

$$\begin{pmatrix} x_4 \\ \theta_4 \end{pmatrix} = B_{44}.f_4 + B_{45}.f_5 \tag{5.5}$$

$$\begin{pmatrix} x_5 \\ \theta_5 \end{pmatrix} = B_{54}.f_4 + B_{55}.f_5 \tag{5.6}$$

where

$$B_{mn} = \begin{bmatrix} D_{mn} \\ S_{mn} \end{bmatrix} \tag{5.7}$$

Connection equations:

$$K_2.(x_4 - x_2) + i.w.C_2.(x_4 - x_2) = f_2 \tag{5.8}$$

$$K_3.(x_5 - x_3) + i.w.C_3.(x_5 - x_3) = f_3 \tag{5.9}$$

and

$$f_2 + f_4 = 0 \tag{5.10}$$

$$f_3 + f_5 = 0 \tag{5.11}$$

combining Equations (5.8) and (5.9)

$$(K_2 + i.w.C_2).(x_4 - x_2) = f_2 \tag{5.12}$$

$$(K_3 + i.w.C_3).(x_5 - x_3) = f_3 \tag{5.13}$$

Substructing Equation (5.3) from (5.5)

$$(x_4 - x_2) = D_{44}.f_4 + D_{45}.f_5 - D_{21}.f_1 - D_{22}.f_2 - D_{23}.f_3 \tag{5.14}$$

Equation (5.4) from (5.6)

$$(x_5 - x_3) = D_{54}.f_4 + D_{55}.f_5 - D_{31}.f_1 - D_{32}.f_2 - D_{33}.f_3 \tag{5.15}$$

Combining Equations (5.10,12 and 14) and also Equations (5.11,13 and 15)

$$f_2 = (K_2 + i.w.C_2)\left(-D_{21}f_1 - (D_{44} + D_{22})f_2 - (D_{45} + D_{23})f_3\right) \tag{5.16}$$

$$f_3 = (K_3 + i.w.C_3)\left(-D_{31}f_1 - (D_{54} + D_{32})f_2 - (D_{55} + D_{33})f_3\right) \tag{5.17}$$

By means these two equations one can write f_2 and f_3 in terms of f_1.

From Equation (5.2)

$$x_1 = D_{11}f_1 + D_{12}f_2 + D_{13}f_3 \tag{5.18}$$

Notice for the assembly

$$X_1 = x_1 \quad \text{and} \quad F_1 = f_1 \tag{5.19}$$

substituting f_2, f_3 and Equation (5.19)in (5.18) the transfer function takes the form of

$$\frac{X_1}{F_1} = D_{11} + \frac{D_{12}}{\dfrac{D_{4523}.D_{5432}}{1/KC_3 + D_{5533}} - \dfrac{1}{KC_2} - D_{4422}} \left(D_{21} - \frac{D_{4523}.D_{31}}{1/KC_3 + D_{5533}} \right) + \frac{D_{13}}{\dfrac{D_{5432}.D_{4523}}{1/KC_2 + D_{4422}} - \dfrac{1}{KC_3} - D_{5533}} \left(D_{31} - \frac{D_{5432}.D_{21}}{1/KC_2 + D_{4422}} \right) \tag{5.20}$$

where

$$KC_2 = K_2 + i.w.C_2 \tag{5.21}$$

$$D_{4523} = D_{45} + D_{23} \tag{5.22}$$

and the other terms in similar manner.

Equation (5.20) relates the deflection of the assembly at point-1 to the force at the same point, by using substructure receptances.

In experiments, the deflection transfer functions of the substructures and assembly are obtained. The connection parameters (K_2, C_2, K_3 and C_3) are determined using *lsqnonlin* command of Matlab Optimization Toolbox**.** *Isqnonlin* solves nonlinear least squares problems, including nonlinear data fitting. *X=lsqnonlin (fnctn,*X_o*)* starts at a point X_0 and finds a minimum to the sum of squares of the functions described in *fnctn*. The solution is always in the specified range *lb* <= *X* <= *ub*. The optimization parameters (*max iteration number, max function evaluation number, tolerances for function and X values*) are specified in the structure options. The value of the residual for a solution *X*, the value *exitflag* (0,1) that describes the exit condition and the structure output that contains information about the optimization are returned.

The frequency response function is in the complex number form, and the equation system obtained is highly nonlinear. This results in a very low computational efficiency. Solution is highly dependent on the initial conditions. When it is tried lowering the tolerances of the function to obtain better results, the code enters in an infinite loop.

It was seen from the modal analysis in CUTPRO that the damping ratio differs with the mode, which means that the damping coefficient also changes. For this reason, the damping coefficient is estimated by the application of a second order polynomial to represent this dependency on frequency.

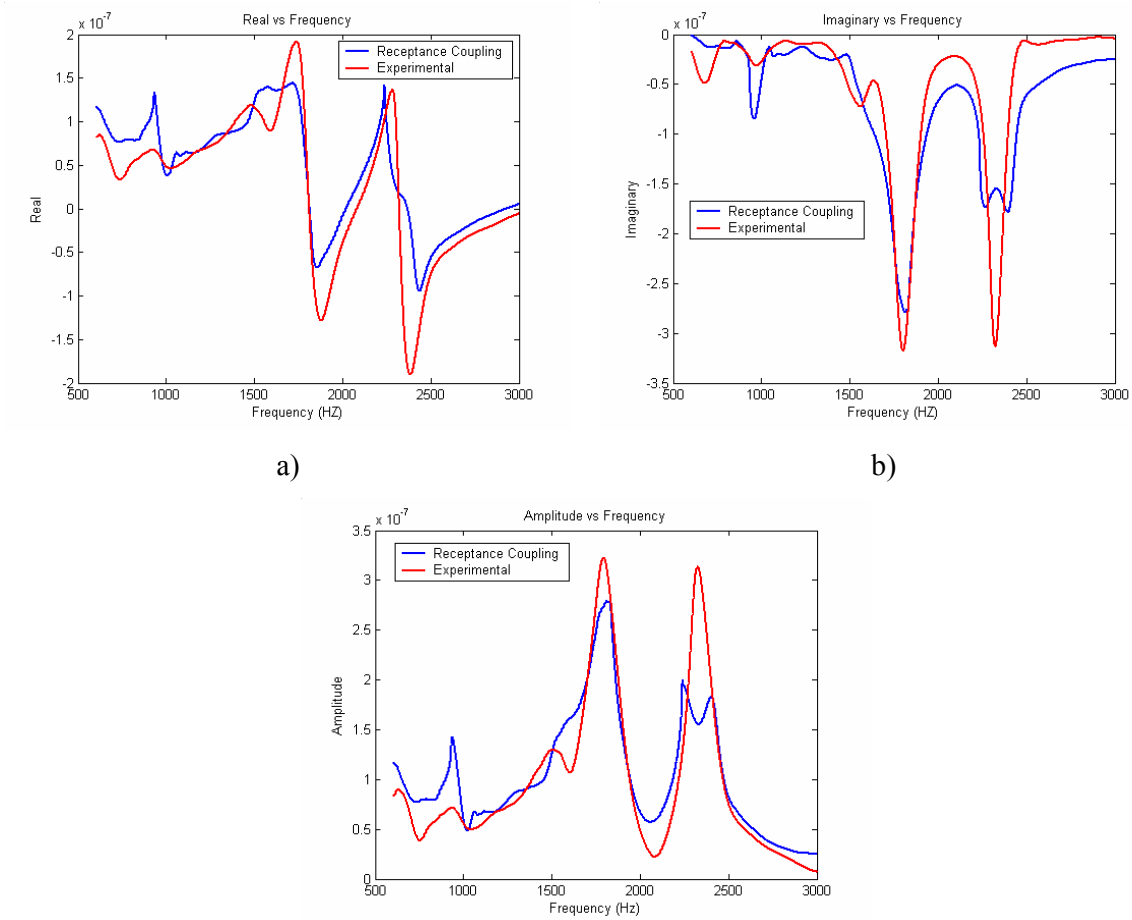

Figure 5.13: a)Real, b)Imaginary, c)Amplitude vs Frequency.

After many runs of the code, it was seen that it gives reasonable results between the frequencies 600-3000 Hz. Even for very different initial conditions, the solutions are close to each other. The best results obtained for the comparison of the real, imaginary parts and amplitude of the FRFs can be seen in Figure 5.13.

Results obtained for the stiffness connection parameters are K_2=9,6e7 N/m and K_3=5,8e7 N/m which are estimated as K_2=2,7e8 N/m and K_3=2,95e8 N/m from the analytical contact models. This study is still going on and the reasons for this difference are investigated. May be the most reasonable explanation of this error is the inaccuracies caused by the manufacturing tolerances. Unlike the assumption of zero clearance used in the modelling, bearings most probably have some clearance. This may cause a big decrease in stiffness as the results obtained. Measurement uncertainties and the numerical errors are the other possible source of error.

The damping coefficient is very difficult to evaluate as it was highly dependent on the initial estimation. In nearly all of the trials, constant term of the second order polynomial estimation always changed, but the coefficients of the second and first order terms seemed to be stabilized. And as a result, the damping coefficient takes the form $C=-54e-5w^2+62e-4w+E$ where w is the vibration frequency and E is any constant.

Consequently, one can say that experimental verification of the rotor model was done, but for the connection stiffness model some problems encountered. It would be better to do the experiments again and improve the code for the estimation of the connection parameters not to come across with computational difficulties. Also for different pre-loads experiments should be implemented and how the parameters change should be followed for the discovery of the new improvements.

6 CONCLUSION

A comprehensive study of rotor dynamics is multidisciplinary since the dynamic behaviour depends also on the behaviour of the bearings and their housings apart from the rotor. In this study, first dynamics of a rotor with classical boundary conditions, then the parameters of the connection stiffness, and finally the influence of these parameters on rotor dynamics were investigated.

With some reasonable assumptions, the bending vibrations of rotors can be reduced to flexural vibrations of static beams. By means of continuity equations coupling of the segments is achieved, and as a result natural frequencies and mode shapes can be determined. Using these characteristics, forced vibration of multi-stepped beams was investigated and an analytic method to obtain the frequency response functions was developed. Damping characteristics of the beam and the supports were also added for the determination of corresponding FRFs.

Proposed rotor model was compared with the finite element analysis for different cases. It was seen that there is a frequency shift problem of the model increasing with the higher modes. This is as a result of neglecting the rotary inertia and shear deformation of the Euler-Bernoulli beam model. To get rid of this Timoshenko beam model, which includes these effects, may be used or a method for the modification of the frequencies should be developed.

The rotor model was also compared with the experiments done with the shaft for free-free boundary conditions. Obtained results showed that apart from the frequency shift, the model estimates the dynamics of the rotor very well. On the other hand, some problems were encountered with the magnitudes of the FRFs for the damped case when it is compared with finite element modelling. Thus, the main reason for this can be concluded to be the different type of modelling of the damping in Femlab.

By means of the application of some contact models nonlinear stiffness characteristics of the connections were determined. The dependency on preload of the bearing stiffness was also investigated. Then the problem turned out to be the

determination of friction coefficient between the housings and the outer races of the bearings since a statically undetermined system emerges. Using the data of a static deformation test a method to obtain this friction coefficient was developed. Results showed that friction coefficient is dependent on the preload applied in the same manner for the common type of bearings. Thus, the determination of the stiffness of a bearing under any preload is proposed.

For the verification of the proposed stiffness model, a substructure analysis applied to the experimental set-up. FRFs to be used in the analysis obtained by dynamic impact tests. Then FRFs of the substructures coupled including the connection parameters in between and equated to the FRF of the whole system. By applying a nonlinear least-square estimation, connection parameters are tried to be determined. Nevertheless, high dependency on the initial conditions and the level of nonlinearity did not make it possible to get reasonably good results, especially for the damping coefficients. The results obtained for stiffness values were less than the estimated ones. Possible reasons of this are the inaccurate manufacturing of the set-up, internal clearance of the bearings and the testing errors.

As a future work one can verify the stiffness model, eliminate the frequency shift problem and develop an optimization algorithm for the preloads and locations of the bearings for the desired dynamic conditions.

REFERENCES

[1] Jerry H. Ginsberg, Mechanical and Structural Vibrations: Theory and Applications, John Wiley, New York, 2001

[2] GMN, Catalogue of High Frequency Spindles for Automatic Tool Change

[3] SK. Jang, CW. Bert, "Free vibrations of stepped beams: exact and numerical solutions," Journal of Sound and Vibration, Vol. 130, No. 2, pp 342-346, 1989

[4] SK. Jang, CW. Bert, "Free vibrations of stepped beams: higher mode frequencies and effects of steps on frequency," Journal of Sound and Vibration, Vol. 132, No. 1, pp 164-168, 1989

[5] S. Naguleswaran, "Vibration of an Euler-Bernoulli beam on elastic end supports and with up to three step changes in cross-section," International Journal of Mechanical Sciences, Vol. 44, pp. 2541-2555, 2002

[6] Hongqi Li, Yung C. Shin, "Integrated Dynamic Thermo-Mechanical Modeling of High Speed Spindles, Part 1: Model Development," Journal of Manufacturing Science and Engineering, Vol. 126, pp 148-158, 2004

[7] Hongqi Li, Yung C. Shin, "Integrated Dynamic Thermo-Mechanical Modeling of High Speed Spindles, Part 2: Solution Procedure and Validations," Journal of Manufacturing Science and Engineering, Vol. 126, pp 159-168, 2004

[8] S. A. Spiewak, T. Nickel, "Vibration based preload estimation in machine tool spindles," International Journal of Machine Tools and Manufacture, Vol. 41, pp. 567-588, 2001

[9] Sun-Min Kim, Sun-Kyu Lee, "Prediction of thermo-elastic behavior in a spindle-bearing system considering bearing surroundings," International Journal of Machine Tools and Manufacture, Vol. 41, pp. 809-831, 2001

[10] S.-M. Kim, S.-K. Lee, K.-J. Lee, "Effect of Bearing Surroundings on the High-Speed Spindle-Bearing Compliance," International Journal of Advanced Manufacturing Technology, Vol. 19, pp. 551-557, 2002

[11] N. Lynagh, H. Rahnejat, M. Ebrahimi, R. Aini, "Bearing induced vibration in precision high speed routing spindles," International Journal of Machine Tools and Manufacture, Vol. 40, pp. 561-577, 2000

[12] N. Aktürk, R. Gohar, "The effect of ball size variation on vibrations associated with ball-bearings," Proceedings of the Institution of Mechanical Engineers, Vol. 212, 1998

[13] Hongqi Li, Yung C. Shin, "Analysis of bearing configuration effects on high speed spindles using an integrated dynamic thermo-mechanical spindle model," International Journal of Machine Tools and Manufacture, Vol. 44, pp. 347-364, 2004

[14] Chi-Wei Lin, Jay F. Tu, Joe Kamman, "An integrated thermo-mechanical-dynamic model to characterize motorized machine tool spindles during very high speed rotation," International Journal of Machine Tools and Manufacture, Vol. 43, pp. 1035-1050, 2003

[15] F. Peeters, R. Pintelon, J. Schoukens, Y. Rolain, E. S. Gutierrez, P. Guillaume, "Identification of Rotor-Bearing Systems in the Frequency Domain Part 1: Estimation of Frequency Response Functions," Mechanical Systems and Signal Processing, Vol. 15, No. 4, pp. 759-773, 2001

[16] F. Peeters, R. Pintelon, J. Schoukens, Y. Rolain, "Identification of Rotor-Bearing Systems in the Frequency Domain Part 2: Estimation of Modal Parameters," Journal of Mechanical Systems and Signal Processing, Vol. 15, No. 4, pp. 775-788, 2001

[17] B. L. Choi, J. M. Park, "Application of the impedance coupling method and the equivalent rotor model in rotor dynamics," Finite Elements in Analysis and Design, Vol. 39, pp. 93-106, 2002

[18] Y. H. Chong, M. Imregun, "Coupling of Non-Linear Substructures using Variable Modal Parameters," Mechanical Systems and Signal Processing, Vol. 14, No. 5, pp. 731-746, 2000

[19] W. Liu, D. J. Ewins, "Substructure Synthesis via Elastic Media Part 2: Coupling Analysis,"

[20] D. J. Ewins, Modal Testing: Theory and Practice, Research Studies Press LTD., 1984

[21] Singerasu S. Rao, Mechanical Vibrations, 3rd Edition, ADDISON-WESLEY, 1995

[22] J. M. Krodkiewski, Lecture Notes on Mechanical Vibration, University of Melbourne, Department of Mechanical and Manufacturing Engineering, 2003

[23] S. Graham Kelly, Fundamentals of Mechanical Vibrations, McGraw-Hill International Editions, 1993

[24] Eugene I. Rivin, Stiffness and Damping in Mechanical Design, Marcel Dekker, Inc., 1999

[25] Alexander H. Slocum, Precision Machine Design, Society of Manufacturing Engineers, 1992

[26] D. Maugis, Contact Adhesion and Rupture of Elastic Solids, Springer, 1998

[27] FEMLAB 3.0a, COMSOL, 2004

[28] Robert D. Blevins, Formulas for Natural Frequency and Mode Shape, Krieger Publishing Company, 2000

[29] Daniel J. Inman, Engineering Vibration, 2nd Edition, Prentice Hall, 2001

[30] FAG, Super Precision Bearings Catalogue

[31] Dynomax Inc., The book of Spindles, Part 1 Spindle Facts, 1st Edition, 2002

[32] CUTPRO® V6.0 Manufacturing Automation Laboratories Inc., 2004

REFERENCES

[1] Jerry H. Ginsberg, Mechanical and Structural Vibrations: Theory and Applications, John Wiley, New York, 2001

[2] GMN, Catalogue of High Frequency Spindles for Automatic Tool Change

[3] SK. Jang, CW. Bert, "Free vibrations of stepped beams: exact and numerical solutions," Journal of Sound and Vibration, Vol. 130, No. 2, pp 342-346, 1989

[4] SK. Jang, CW. Bert, "Free vibrations of stepped beams: higher mode frequencies and effects of steps on frequency," Journal of Sound and Vibration, Vol. 132, No. 1, pp 164-168, 1989

[5] S. Naguleswaran, "Vibration of an Euler-Bernoulli beam on elastic end supports and with up to three step changes in cross-section," International Journal of Mechanical Sciences, Vol. 44, pp. 2541-2555, 2002

[6] Hongqi Li, Yung C. Shin, "Integrated Dynamic Thermo-Mechanical Modeling of High Speed Spindles, Part 1: Model Development," Journal of Manufacturing Science and Engineering, Vol. 126, pp 148-158, 2004

[7] Hongqi Li, Yung C. Shin, "Integrated Dynamic Thermo-Mechanical Modeling of High Speed Spindles, Part 2: Solution Procedure and Validations," Journal of Manufacturing Science and Engineering, Vol. 126, pp 159-168, 2004

[8] S. A. Spiewak, T. Nickel, "Vibration based preload estimation in machine tool spindles," International Journal of Machine Tools and Manufacture, Vol. 41, pp. 567-588, 2001

[9] Sun-Min Kim, Sun-Kyu Lee, "Prediction of thermo-elastic behavior in a spindle-bearing system considering bearing surroundings," International Journal of Machine Tools and Manufacture, Vol. 41, pp. 809-831, 2001

[10] S.-M. Kim, S.-K. Lee, K.-J. Lee, "Effect of Bearing Surroundings on the High-Speed Spindle-Bearing Compliance," International Journal of Advanced Manufacturing Technology, Vol. 19, pp. 551-557, 2002

[11] N. Lynagh, H. Rahnejat, M. Ebrahimi, R. Aini, "Bearing induced vibration in precision high speed routing spindles," International Journal of Machine Tools and Manufacture, Vol. 40, pp. 561-577, 2000

[12] N. Aktürk, R. Gohar, "The effect of ball size variation on vibrations associated with ball-bearings," Proceedings of the Institution of Mechanical Engineers, Vol. 212, 1998

[13] Hongqi Li, Yung C. Shin, "Analysis of bearing configuration effects on high speed spindles using an integrated dynamic thermo-mechanical spindle model," International Journal of Machine Tools and Manufacture, Vol. 44, pp. 347-364, 2004

[14] Chi-Wei Lin, Jay F. Tu, Joe Kamman, "An integrated thermo-mechanical-dynamic model to characterize motorized machine tool spindles during very high speed rotation," International Journal of Machine Tools and Manufacture, Vol. 43, pp. 1035-1050, 2003

[15] F. Peeters, R. Pintelon, J. Schoukens, Y. Rolain, E. S. Gutierrez, P. Guillaume, "Identification of Rotor-Bearing Systems in the Frequency Domain Part 1: Estimation of Frequency Response Functions," Mechanical Systems and Signal Processing, Vol. 15, No. 4, pp. 759-773, 2001

[16] F. Peeters, R. Pintelon, J. Schoukens, Y. Rolain, "Identification of Rotor-Bearing Systems in the Frequency Domain Part 2: Estimation of Modal Parameters," Journal of Mechanical Systems and Signal Processing, Vol. 15, No. 4, pp. 775-788, 2001

[17] B. L. Choi, J. M. Park, "Application of the impedance coupling method and the equivalent rotor model in rotor dynamics," Finite Elements in Analysis and Design, Vol. 39, pp. 93-106, 2002

[18] Y. H. Chong, M. Imregun, "Coupling of Non-Linear Substructures using Variable Modal Parameters," Mechanical Systems and Signal Processing, Vol. 14, No. 5, pp. 731-746, 2000

[19] W. Liu, D. J. Ewins, "Substructure Synthesis via Elastic Media Part 2: Coupling Analysis,"

[20] D. J. Ewins, Modal Testing: Theory and Practice, Research Studies Press LTD., 1984

[21] Singerasu S. Rao, Mechanical Vibrations, 3rd Edition, ADDISON-WESLEY, 1995

[22] J. M. Krodkiewski, Lecture Notes on Mechanical Vibration, University of Melbourne, Department of Mechanical and Manufacturing Engineering, 2003

[23] S. Graham Kelly, Fundamentals of Mechanical Vibrations, McGraw-Hill International Editions, 1993

[24] Eugene I. Rivin, Stiffness and Damping in Mechanical Design, Marcel Dekker, Inc., 1999

[25] Alexander H. Slocum, Precision Machine Design, Society of Manufacturing Engineers, 1992

[26] D. Maugis, Contact Adhesion and Rupture of Elastic Solids, Springer, 1998

[27] FEMLAB 3.0a, COMSOL, 2004

[28] Robert D. Blevins, Formulas for Natural Frequency and Mode Shape, Krieger Publishing Company, 2000

[29] Daniel J. Inman, Engineering Vibration, 2nd Edition, Prentice Hall, 2001

[30] FAG, Super Precision Bearings Catalogue

[31] Dynomax Inc., The book of Spindles, Part 1 Spindle Facts, 1st Edition, 2002

[32] CUTPRO® V6.0 Manufacturing Automation Laboratories Inc., 2004